MICROCOPY RESOLUTION TEST CHART
NATIONAL BUREAU OF STANDARDS-1963-A

LEVEL

NAVAL POSTGRADUATE SCHOOL
Monterey, California

DTIC
SELECTED
MAR 1 0 1980

A

A PRIMITIVE VARIABLE MATHEMATICAL
MODEL FOR PREDICTING THE FLOWS
IN TURBOJET TEST CELLS

Charles A. Stevenson
and
David W. Netzer

October 1979

80 3 10 017

ADA081539

DDC FILE COPY

NAVAL POSTGRADUATE SCHOOL

Monterey, California

Rear Admiral T. F. Dedman
Superintendent

Jack R. Borsting
Provost

Reproduction of all or part of this report is authorized.
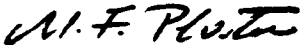
This report was prepared by:

CHARLES A. STEVENSON
LT, US NAVY

DAVID W. NETZER
Associate Professor of
Aeronautics

Reviewed by:

Released by:

M. F. PLATZER, Chairman
Department of Aeronautics

W. M. TOLLES
Dean of Research

EMB REPORT DOCUMENTATION PAGE	READ INSTRUCTIONS BEFORE COMPLETING FORM

1. REPORT NUMBER NPS67-79-009	2. GOVT ACCESSION NO.	3. RECIPIENT'S CATALOG NUMBER

4. TITLE (and Subtitle) A Primitive Variable Mathematical Model for Predicting the Flows in Turbojet Test Cells	5. TYPE OF REPORT & PERIOD COVERED Final Report 1979
	6. PERFORMING ORG. REPORT NUMBER

7. AUTHOR(s) Charles A. Stevenson and David W. Netzer	8. CONTRACT OR GRANT NUMBER(s)

9. PERFORMING ORGANIZATION NAME AND ADDRESS Naval Postgraduate School Monterey, CA 93940	10. PROGRAM ELEMENT, PROJECT, TASK AREA & WORK UNIT NUMBERS N6237679WR00014

11. CONTROLLING OFFICE NAME AND ADDRESS Naval Air Propulsion Center Trenton, NJ	12. REPORT DATE October 1979
	13. NUMBER OF PAGES 61

14. MONITORING AGENCY NAME & ADDRESS(if different from Controlling Office)	15. SECURITY CLASS. (of this report) Unclassified
	15a. DECLASSIFICATION/DOWNGRADING SCHEDULE

16. DISTRIBUTION STATEMENT (of this Report)

Approved for public release; distribution unlimited.

17. DISTRIBUTION STATEMENT (of the abstract entered in Block 20, if different from Report)

18. SUPPLEMENTARY NOTES

19. KEY WORDS (Continue on reverse side if necessary and identify by block number)

Turbojet Test Cells
Computer Model

20. ABSTRACT (Continue on reverse side if necessary and identify by block number)

An adaptation of a primitive variable, finite-difference computer program was made in order to predict the non-reacting flow fields in turbojet test cells. The study compares the predictions of the primitive variable computer model with an earlier stream function-vorticity computer model and empirical data. It was found that the model reasonably predicted the flow fields and allowed simulation of test cell flows up to full engine throttle conditions.

DD FORM 1473 EDITION OF 1 NOV 65 IS OBSOLETE
1 JAN 73
S/N 0102-014-6601

i

251450

TABLE OF CONTENTS

Page

LIST OF FIGURES

Page

v

LIST OF TABLES

ABBREVIATIONS AND SYMBOLS

ROMAN SYMBOLS

A   Area

$\left.\begin{array}{l} C_1 \\ C_2 \\ C_D \end{array}\right\}$ K-ε model empirical constants (Table I)

C_p Specific heat at constant pressure

E   9.0

h   Enthalpy

$\tilde{h}$ Stagnation enthalpy

I   Turbulence intensity

K,k Turbulence kinetic energy

$\bar{M}$ Average molecular weight

P,p Pressure

r   Radial distance

R   Gas constant

$\bar{R}$ Universal gas constant

S   Source terms

T   Temperature

u   Axial velocity

v   Radial velocity

x   Axial distance

y_p^+ Dimensionless distance from solid boundary

GREEK SYMBOLS

Γ Effective transport coefficient

δ Incremental distance from wall

ϵ Turbulence dissipation rate

κ von Karman constant

μ Viscocity

ρ Density

σ Prandtl or Schmidt Number

τ Shear stress

ϕ Any variable

SUBSCRIPTS

eff   Effective

lam   Laminar

p   Near wall node

t   Turbulent

w   wall

I. INTRODUCTION

During the past few years, there have been many advancements in numerical techniques for predicting the behavior of fluid flows. For example, several computer models have been developed by Gosman, Spalding and others [1,2,3] which use the mass, momentum and energy conservation equations reduced to finite difference, nonlinear algebraic form. The development of reliable computer programs of this type greatly benefits engineering analysis in such widely varying fields as meteorology, aerodynamics and gasdynamics.

The earlier two-dimensional computer codes were based on vorticity (ω) and stream function (ψ) [1,2,5]. This form of the governing equations eliminates pressure and velocity from immediate consideration. Pressure is normally calculated only after a converged solution is obtained. This technique has several inherent disadvantages:

1. It results in large errors in the predicted pressure distributions in all but quiescent flow regions due to the higher order dependence of the pressure gradient on stream function [6].

2. It is usually restricted to constant density flows or to flows in which density varies only with temperature [3,6].

3. The boundary conditions are difficult to specify [3,5]

4. Considerable difficulty has been experienced in arriving at converged solutions, especially for non-uniformly

1

spaced grids and high flow rates [2,5,6,7].

5. The ψ-ω model is not easily extended to three-dimensional flows [3].

To overcome these difficulties, emphasis has been placed on developing computer codes based on velocity and pressure, the primitive variables.

A major problem with any new computer model is model validation. The difficulties of collecting accurate empirical data are multiplied when investigating three-dimensional and/or reacting flows. In addition, many variables within these flows are not readily measurable (turbulence intensities, etc.).

An effort to utlize elliptic computer models which can handle turbulent, reacting, variable density flows at high subsonic and sonic velocities has been underway at the Naval Postgraduate School for several years. Two specific areas which have been investigated are flows in a turbojet test cell and in the combustion environment of a solid fuel ramjet.

It is important to have the capability to test high performance jet engines throughout their operating envelope under conditions which approximate installed conditions. This is often accomplished in blockhouse type installations called turbojet test cells (TJTC). The typical test cell incorporates an inlet, a horizontal test section and a vertical exhaust stack. The engine to be tested is normally mounted near the center of the cell to allow the development of a nearly uniform engine inlet velocity profile. The engine exhausts into an augmentor tube which entrains additional air for exhaust gas cooling and dilution. The quantity of this secondary air is

crucial to proper engine testing and test cell performance.

Testing today's high power and high mass flow engines in these installations produces a myriad of noise and air pollution problems. Cell modifications must often be made to minimize these problems. This fact coupled with the future need for larger, more expensive test cells to replace obsolete cells and to accommodate new generations of high technology engines, makes the development of reliable modeling methods imperative. The frequently used one-dimensional models are not adequate for predicting the details of the complicated flows within a turbojet test cell and, therefore, the cells often do not perform to their designed limits. An accurate flow model would provide a needed design tool which could help prevent costly design errors and improve operating efficiency.

A two-dimensional $\psi-\omega$ computer code was used to analyze the flows in a full scale and a subscale turbojet test cell at the Naval Postgraduate School [2,6]. Experimental data from the subscale test cell have been compared with computations made with this computer model [6]. A primitive variable (u-v-p) computer model could improve this capability by extending it to specific geometries and flow rates that the $\psi-\omega$ model was incapable of predicting. In addition, a u-v-p model would more readily allow variable density flows to be analyzed and should more accurately predict augmentor pressure distribution. An application of a primitive variable model to jet pumps has been reported by Croft and Lilley [4].

3

The primary objective of this investigation was to adapt a primitive variable model to the turbojet test cell geometry and flow conditions and to validate that model with data from a subscale turbojet test cell. Possible utilization of the model for predicting optimum placement of sound suppressors/ jet break-up devices within the augmentor tube was also investigated.

II. MODEL OVERVIEW

A. INTRODUCTION

The computer model used in this study was adapted from the CHAMPION 2/E/FIX computer program developed by Pun and Spalding [8]. CHAMPION is a TWO-dimensional Elliptic, FIXed grid computer program which provides a solution of the conservation equations for recirculating flows in finite difference form.

B. ASSUMPTIONS

The flow was assumed to be steady, two-dimensional and subsonic. For simplicity the value of specific heat (C_p) was assumed to be constant although its dependence on temperature and/or composition could easily be included.

A modified Jones-Launder [8,10,11,12] two parameter turbulence model was incorporated to calculate the effective viscosity. It uses five empirical constants (Table I) and requires that two additional variables, turbulence kinetic energy (K) and turbulence dissipation rate (ϵ), be evaluated. Effective viscosity was calculated using the formulas:

$$\mu_{eff} = \mu_{lam} + \mu_t \tag{1}$$

where

$$\mu_t = C_D \, \rho \, K^2/\epsilon \tag{2}$$

The turbulent Prandtl and Schmidt numbers were taken equal to unity and, therefore, the turbulent Lewis number was

5

C_1	C_2	C_D	$\sigma_{k,eff}$	$\sigma_{\varepsilon,eff}$
1.43	1.92	0.09	1.0	1.3

TABLE I. $K-\varepsilon$ TURBULENCE MODEL EMPIRICAL CONSTANTS

unity [9]. The laminar Prandtl number was also taken to be unity.

C. GOVERNING EQUATIONS

The conservation equations for axi-symmetrical flows with no tangential variations can be put into the general form [8].

$$\frac{\partial}{\partial x}(\rho u\phi) + \frac{1}{r}\frac{\partial}{\partial r}(\rho r v\phi) - \frac{\partial}{\partial x}(\Gamma_\phi \frac{\partial \phi}{\partial x}) - \frac{1}{r}\frac{\partial}{\partial r}(r\Gamma_\phi \frac{\partial \phi}{\partial r}) = S_\phi \quad (3)$$

convection terms   diffusion terms   source terms

where ϕ stands for the dependent variable $(u,v,k,\epsilon,\tilde{h}$, etc.) being considered ($\phi = 1$ for the continuity equation), Γ_ϕ is the appropriate effective exchange coefficient for turbulent flow and S_ϕ is the "source term" (Table II). The energy equation in terms of stagnation enthalpy has no source terms since the turbulent Prandtl and Schmidt numbers were chosen as unity and radiative transport was neglected [1,3]. Thus the stagnation enthalpy is given by:

$$\tilde{h} = h + (u^2 + v^2)/2 + K \quad (4)$$

where for non-reacting flows:

$$h = C_p T \quad (5)$$

The calculation of temperature was made using equations (4) and (5). Density was calculated from the perfect gas law:

$$\rho = P/RT \quad (6)$$

where $R = \bar{R}/\bar{M}$ (7)

7

ϕ	Γ_ϕ	S_ϕ
u	μ_{eff}	$-\dfrac{\partial P}{\partial x} - \dfrac{2}{3}\dfrac{\partial}{\partial x}[\dfrac{\mu}{r}(\dfrac{\partial}{\partial x}(ru) + \dfrac{\partial}{\partial r}(rv))] + \dfrac{\partial}{\partial x}(\mu\,\dfrac{\partial u}{\partial x}) + \dfrac{1}{r}\dfrac{\partial}{\partial r}\,(\mu r\,\dfrac{\partial v}{\partial x})$
v	μ_{eff}	$-\dfrac{\partial P}{\partial r} - 2\,\dfrac{\mu v}{r^2} - \dfrac{2}{3}\dfrac{2}{r}\dfrac{\partial}{\partial r}\{\dfrac{\mu}{r}[\dfrac{\partial}{\partial x}(ru) + \dfrac{\partial}{\partial r}(rv)]\} + \dfrac{\partial}{\partial x}(\mu\,\dfrac{\partial u}{\partial r}) + \dfrac{1}{r}\dfrac{\partial}{\partial r}(\mu r\,\dfrac{\partial v}{\partial r})$
TKE	μ_{eff}/σ_k	$\mu_t\,(2[(\dfrac{\partial u}{\partial x})^2 + (\dfrac{\partial v}{\partial r})^2 + (\dfrac{v}{r})^2] + (\dfrac{\partial u}{\partial r} + \dfrac{\partial v}{\partial x})^2) - \rho\epsilon$
TED	$\mu_{eff}/\sigma_\epsilon$	$\dfrac{C_1\epsilon}{k}(\mu_t\,(2[(\dfrac{\partial u}{\partial x})^2 + (\dfrac{\partial v}{\partial r})^2 + (\dfrac{v}{r})^2] + (\dfrac{\partial u}{\partial r} + \dfrac{\partial v}{\partial x})^2)) - \dfrac{C_2\rho\epsilon^2}{k}$
$\tilde{h}$	μ_{eff}/σ_h	0

$\sigma_j = \sigma_k = \sigma_h = 1 \,, \quad \sigma_\epsilon = 1.3$

$C_1 = 1.43 \quad C_2 = 1.92 \quad v_\theta = 0$

TABLE II. GOVERNING EQUATION PARAMETERS

D. CONSERVATION OF MASS

On each radial line the mass flow rate was calculated using the local density. The error in mass flow (compared to the summation of "mass-in" at all upstream boundaries) was used to uniformly adjust the axial velocity over the entire line. This process ensured that overall continuity was satisfied on the line. The pressure at all downstream locations was then adjusted to approximately correct for the momentum imbalance created by the uniform axial velocity adjustment. A "pressure correction" equation was then solved for each cell on the line. Local cell velocity (axial and radial) and pressure were then adjusted to satisfy cell-wise continuity. The details of this procedure are presented in reference 8.

E. BOUNDARY CONDITIONS

1. Introduction

Fixed boundary conditions were set at the desired or experimentally determined value and held constant. Specified gradient boundary conditions were handled by setting the appropriate convection/diffusion coefficient to zero in the finite difference equation ("breaking the link") and then entering the appropriate gradient through linearized "false" source terms [8]. The geometry and appropriate boundary conditions for the test cell are summarized in figure 1.

2. Inlet

Although not a computer program limitation, "plug flow" was assumed at the nozzle exit and cell inlet planes. The (secondary) flow inlet of the TJTC was recessed approximately 0.3 meters (figure 1) to allow a velocity profile to

9

develop over the length of the engine. Turbulence kinetic energy was selected to be uniform with a value which corresponded to the approximate turbulence intensity of the inlet flow.

3. Axis of Symmetry and Exit Plane

Radial and axial gradients were set equal to zero on the center line and exit respectively. The radial flow velocity was equated to zero.

4. Solid Boundaries

All solid boundaries were considered adiabatic with both velocity components equal to zero ("no slip" condition).

For simplicity, a two part boundary layer was used. The border between the laminar sublayer and the turbulent layer was taken at $y_p^+ = 11.5$ [8]. y_p^+ was evaluated at each near wall node (p),

$$y_p^+ = (\rho\delta/\mu_{lam})(\tau_w/\rho)^{1/2} \qquad (8)$$

where, for $y_p^+ \geq 11.5$

$$\tau_w = C_D^{1/2} \rho K_p \qquad (9)$$

τ_w was assumed uniform from the wall to the near wall grid point. Thus,

$$y_p^+ = C_D^{1/4} \rho K_p^{1/2} \delta/\mu_{lam} \qquad (10)$$

If $y_p^+ \geq 11.5$, the wall shear stress (τ_w) was calculated using the formula:

$$\tau_w = C_D^{1/2} \rho K_p = \rho C_D^{1/4} K_p^{1/2} (u/u^+) \tag{11}$$

$$= \kappa C_D^{1/4} \rho u_p K_p^{1/2}/\ln(E\rho\delta C_D^{1/4} K_p^{1/2}/\mu_{lam})$$

where

$$u^+ \equiv \frac{1}{\kappa} \ln(E\, y_p^+) \tag{12}$$

Wall shear stress was evaluated for $y_p^+ < 11.5$ from the formula:

$$\tau_w = \mu_{lam}\, u_p/\delta \tag{13}$$

Due to the steep gradients of properties in turbulent flows near solid boundaries, the source terms for K and ϵ at near wall nodes were expressed in terms of the wall shear stress [1,8]. τ_w also provides the boundary condition for the u and v equations. In the following equation for turbulence dissipation rate (ϵ) at a near wall node (p), the length scale is presumed proportional to the distance from the wall (δ).

$$\epsilon_p = C_D^{3/4} K_p^{3/2}/\kappa\delta = K_p^{3/2}/2.43\delta \tag{14}$$

Equation (13) implies that the wall shear stress is calculated assuming a linear velocity profile when $y_p^+ < 11.5$. A near-wall grid point, therefore, can lie within the laminar sublayer, but the source terms for K and ϵ imply that μ_{eff}/μ_{lam} is

11

much greater than one [10,11]. This fact precludes y_p^+ from being significantly less than 11.5.

F. SOLUTION PROCEDURE

Five variables (u,v,K,ε and $\tilde{h}$) were solved using equation (3) in finite difference form. The line by line iterative procedure employed upwind differencing and under relaxation to promote convergence [8]. Pressure (relative to a selectable position and magnitude within the grid) was obtained from the mass conservation imposed on each radial grid line and on each nodal control volume as discussed above. Effective viscosity, temperature and density were also obtained as described above. A more detailed explanation of this procedure can be found in reference 8.

III. TURBOJET TEST CELL NOISE CONSIDERATIONS

A. INTRODUCTION

Lighthill [13] and others have built a general physical theory of aerodynamic sound production. He has also specialized that theory to the study of turbulence as a source of sound [14]. Experiments have shown [14] that aerodynamic noise generated by a subsonic cold jet in the absence of any fluctuating forces between the fluid and solid boundaries exhibits the following characteristics:

(1) The acoustic power output varies as a high power (near the eighth) of the jet velocity.

(2) A very broad spectrum with a peak frequency near $U^2/2d$, where U is the jet velocity and d the nozzle diameter.

(3) Almost all the sound is radiated in directions making an acute angle with the jet axis.

(a) Higher frequencies, which are apparently emitted mainly from the vicinity of the nozzle exhaust plane, are radiated at an angle of 45°, or slightly less, to the jet axis.

(b) Lower frequencies, which are apparently emitted from the jet five to twenty diameters downstream of the nozzle, are radiated at much smaller angles.

Lighthill postulated [14] that the high frequency sound emanates from the heavily sheared mixing region near the nozzle exhaust and that the low frequency emanates from the region of more nearly isotropic turbulence farther downstream in the core

13

of the jet.

While a myriad of research has been done on the generation
and propagation of noise from a free jet, little research has
been directed toward the problem of aerodynamic noise produced
by confined jets. The propagation of sound associated with
this type of flow is significantly more complicated due to the
close proximity of several fixtures which absorb or reflect
sound in varying degrees. In a turbojet test cell the engine
is tested in close proximity to an augmentor tube which is
used for mixing and cooling the exhaust gases before they are
vented to the atmosphere through a stack. Each of these struc-
tures influences the sound propagation in some way.

The numerical models discussed above can be used to predict
velocity, pressure and turbulence intensity distributions in
confined turbulent flows like those discussed above. It may
be possible to use the computer codes to predict optimum place-
ment of sound suppressors in geometrically complicated flows
like those in a turbojet test cell.

An attempt was made to measure the sound produced within
the Naval Postgraduate School subscale turbojet test cell aug-
mentor tube. These data were compared to the flow field pre-
dictions obtained with the computer model.

B. EXPERIMENTAL APPARATUS

1. Test Cell

Design and construction of the NPS subscale turbojet
test cell are detailed in reference 15. The cell is a one-

14

eighth scale model of a NAS Alameda test cell. A TF 41 engine was scaled to one-eighth in diameter resulting in the mass flow being scaled by one-sixty fourth to maintain flow velocities equal to those in the full scale cell. The test section is enclosed by hinged plexiglas sides to allow easy access and visual monitoring of the section during operation. These sides were held open during the acoustic measurements described in this report. The augmentor tube, equipped with a straight inlet, exits the cell through a removable wall. Its downstream end is normally attached to a deflector-plate-equipped vertical exhaust stack. For this experiment, however, the stack was removed, allowing the fluid exiting the augmentor tube to vent to the atmosphere. In an effort to reduce sound reflection inside the test cell, a one-quarter inch plywood divider with three-quarter inch foam padding was extended from the augmentor inlet to the plexiglas sides of the test cell.

The combustor used to simulate turbojet tailpipe and nozzle conditions was supplied with compressed air from an Allis-Chalmers, twelve stage axial compressor. The tailpipe was fitted with either a small (2 inches diameter) or large (3.5 inches diameter) nozzle.

2. Instrumentation

Several methods were employed in an attempt to measure the aerodynamic noise generated by the engine exhaust in the subscale test cell. The proximity of various structures including the augmentor tube and the stack produced an "acoustically dirty" environment. This prevented useful data from being taken external to the augmentor tube regardless of the pressure

15

transducer orientation to, or distance from the jet axis. The method chosen to obtain these measurements is illustrated in figure 2.

The top of the augmentor tube incorporated a series of pressure taps. Several of these were modified to accept a one-eighth inch directional microphone. The microphone was inserted flush with the inside of the augmentor tube. Initially it was held in a plexiglas plug with a set screw (figure 2). The transducer signals were amplified, displayed and recorded using a Spectral Dynamics Corporation model 50330 spectrum analyzer and a HP 7035B X-Y recorder.

After initial testing an attempt was made to isolate those frequencies associated with the physical resonance of the augmentor tube and test cell from those generated directly from the jet mixing process. The pressure transducer was wrapped with styrofoam and refitted in the plexiglas holder without the securing set screw. To determine the degree to which the adjacent building was contributing to the recorded data, a plywood sheet was positioned between the cell and building.

C. DATA ACQUISITION AND REDUCTION

Sufficient data were recorded for each test condition to allow the mass flow rates for the nozzle, test cell and augmentor tube to be calculated. In addition, a plot of frequency vs sound intensity was recorded at each of the seven augmentor ports. On subsequent runs with the modified transducer holder and alternate background, data were recorded under similar conditions at augmentor port number four only.

16

D. COMPUTER MODEL PREDICTIONS

At attempt was not made to predict the sound distribution within the augmentor tube. Rather the velocity, pressure and turbulence kinetic energy distributions were calculated using the computer program discussed above. It was desired to determine whether these distributions could be used as a first approximation for locating the peak noise intensities within the augmentor tube.

IV. DISCUSSION OF RESULTS

A. INTRODUCTION

The purpose of this study was to utlize a primitive vari-
able, finite difference computer program to analyze the flow
within a turbojet test cell and to validate the model with data
obtained from a subscale turbojet test cell located at the
Naval Postgraduate School. Previous work [2,6,7] had accom-
plished this task for a ψ-ω computer model and, therefore,
empirical data and the predictions of the ψ-ω model were avail-
able for comparison. The experimental data available consisted
of augmentor wall pressure distributions and radial velocity
profiles along the length of the augmentor tube for low, medium,
and high engine flow rates.

As previously indicated, the ψ-ω model did a poor job of
predicting pressure distributions in all but quiescent flow re-
gions. Additionally, numerical convergence was difficult to ob-
tain with that model when used to predict high velocity flows
where compressibility effects are significant. It was antici-
pated that a primitive variable model would help to alleviate
these difficulties. It is desirable to have a model which can
be used to predict the flow field for full-throttle engine con-
ditions where the engine exhaust flow is choked.

Adaptation of the primitive variable model to the subscale
test cell geometry required the use of several approximations:

(1) In modeling axi-symmetric flow, the engine was by
necessity positioned at the axis of symmetry. In the actual
test cell the engine was mounted closer to the deck than to

the overhead. It would be expected, therefore, that the velocity distribution in the secondary flow (the flow around the engine) would be somewhat different than predicted.

(2) The subscale test cell cross section was rectangular while the engine and augmentor tube were cylindrical. The system was modeled as three concentric cylinders with cross-sectional areas equivalent to the physical system. The nozzle exit area, the test section cross-sectional area and the empirical augmentation ratios and mass flow rates were used in calculating the axial inlet velocities used in both computer models.

(3) The actual engine incorporated a converging nozzle. The engine was modeled as a cylinder with a diameter equal to the actual nozzle exhaust diameter.

(4) In the model the augmentor inlet and the aft test cell wall were taken to be flush. The actual augmentor is often inserted into the test section which forms a recirculation zone above the augmentor tube. The effects on the augmentor flow field introduced by this recirculation region have been shown to be minimal [7]. It should be noted that the $\psi-\omega$ model incorporated this recirculation zone and a flow reducing lip flange on the augmentor inlet. When comparisons were made between the predictions of the two models, the effects of this recirculation zone and the augmentor inlet lip flange in the $\psi-\omega$ model were minimized by reducing their dimensions to one grid spacing.

There was one additional difference between actual test conditions and the numerical model. In a test cell of specified geometry (cross-sectional area, inlet and stack acoustic

19

and pollution treatment devices, augmentor tube length, diameter and inlet geometry, etc.) the mass flow rate of secondary air pumped by the engine exhaust and the pressure distribution throughout the cell are unique functions of the engine flow rate. The static pressures at the cell inlet and stack exhaust are both equal to the local atmospheric pressure. Thus, the most desirable model capability would be the prediction of the cell flow field as a function only of engine flow rate. To accomplish this with a two-dimensional finite-difference model would greatly complicate the analysis and increase the required computer computation time. In this investigation the flow field was predicted only for the test cell flow from the engine inlet to the exhaust of the augmentor tube. Since inlet boundary conditions are required for the solution of the elliptic equations, the mass flow rate of secondary air was specified at the experimentally measured valve. The predicted pressure profiles were then compared to the measured values. An alternate method could have been employed, requiring significantly greater computer time: iterate on the inlet mass flow rate until a specified augmentor exhaust pressure was attained.

Three of the flow conditions selected for model validation corresponded to conditions where empirical data were available. Model predictions for two additional conditions were made increasing the engine-to-augmentor inlet spacing to one and two engine diameters. No empirical data were available for the two latter conditions and, therefore, inlet parameters were simulated using empirical data for zero engine-

to-augmentor entrance spacing. The test conditions are summarized in Table III.

Figures 3 through 7 compare predicted axial pressure distributions and radial velocity profiles obtained with the ψ-ω and u-v-p computer models. In addition, the available empirical data are also plotted on those figures. The velocity profiles from both computer models were plotted for the grid lines closest to the locations of the experimental data. In the cases where empirical data were not available, various representative velocity profiles were plotted for both models. Experimental pressure profiles were available only on the deck of the test cell and along the top of the augmentor tube. Thus, for negative positions in Figures 3 through 7 no empirical data were available for direct comparison to the predicted profiles. The models did predict a very small pressure drop along the test cell deck in agreement with experiment. Predicted axial pressure profiles are presented for various radial positions. These locations are given as fractions of augmentor tube radius (R_a). For example, the pressure distribution labeled $R = 0.96\ R_a$ indicates that the distribution is along an axial grid line located at a distance 96 percent of the augmentor radius from the axis of symmetry. Two ψ-ω model axial pressure profiles are depicted for each test condition. One profile $(R = 0.38\ R_a)$ lies in the quiescent flow region between the engine and augmentor and was previously found by Walters [6] to be the only location which produced a reasonable estimate of the measured profiles. The second axial pressure

21

CASE	$\dot{m}_e$ [kg/sec]	A.R.	Engine-augmentor Spacing [M]	P_{in}^* [N/M^{2}x10^{-5}]	P_e^{**} [N/M^{2}x10^{-5}]	T_{in}^* [°K]	T_e^{**} [°K]	u_e^{**} [m/sec]
I	0.45	2.26	0	1.013	1.013	288.9	287.8	187.8
IIA	0.69	3.12	0	1.010	1.010	289.4	270.0	272.5
IIB	0.69	3.12	0.05	1.010	1.010	289.4	270.0	272.5
IIC	0.69	3.12	0.10	1.010	1.010	289.4	270.0	272.5
III	0.99	2.89	0	1.009	1.242	289.4	263.9	310.0

*Test cell at engine inlet

**Nozzle exhaust

TABLE III. TURBOJET TEST CELL TEST CONDITIONS

distribution $(R = 0.13 R_a)$ was located at less than one
engine radius of the center line. Three u-v-p model axial
pressure profiles are presented for each test condition. One
distribution $(R = 0.04 R_a)$ is near the axis of symmetry.
Another profile $(R = 0.28 R_a)$ runs along the top of the
engine and through the turbulent mixing region. The third
profile $(R = 0.96 R_a)$ is close to the augmentor wall.

B. RESULTS AND DISCUSSION - PRESSURE AND VELOCITY DISTRIBUTIONS

    1. <u>Test Case I - Low Flow Rate/Zero Spacing</u>

        a. Velocity Profiles

            Both models predicted virtually identical velocity
profiles at each station along the augmentor tube (Figure 3).
There was close agreement between the predicted and the experi-
mental velocity profiles at the exit of the augmentor. The
latter result was expected since the velocity profile had be-
come fully developed near the augmentor exit.

        b. Pressure Profiles

            (1) $\psi-\omega$ Model. This test condition had the
lowest flow rates and offered the best chance for agreement
with experiment. The initial pressure drop and the pressure
rise were underpredicted in the outer flow region $(R = 0.38 R_a)$.
Nearer the axis of symmetry $(R = 0.13 R_a)$ the initial pressure
decrease was significantly overpredicted, but the magnitude
(from minimum to maximum) and profile of the pressure rise were
in good agreement with the experimental wall profile. The pre-
dicted pressure curves leveled off earlier than the experimental
data. The difficulty in obtaining good pressure profiles with
this model are evident. Near the augmentor exit there should

23

be negligible radial pressure variations. The solution was converged in all dependent variables (Table V) and negligible pressure variation was calculated in the radial direction near the augmentor exit. However, the pressure profiles along the two axial paths (calculated by summing $(\partial p/\partial x) \cdot \Delta x$ from the inlet end) did not become equal near the augmentor exit. The latter resulted from the large errors in the predicted profiles near the augmentor inlet (i.e., $\frac{\partial p}{\partial x}$ in the expression $P_x - P_{ref} = \sum_{x=0} (\frac{\partial p}{\partial x}) \Delta x$ is very inaccurate near the augmentor inlet). This difficulty with the $\psi-\omega$ model has been previously discussed by Walters and Netzer [6].

(2) u-v-p Model. Both the pressure drop and rise within the augmentor were underpredicted. However, the primitive variable model more accurately predicted the location of the minimum pressure and seemed to level off at approximately the same augmentor position as the experimental data. Walters and Netzer [6] have previously shown that the models predict that mixing is nearly complete at the location where the pressure profile levels off (and simultaneously, where the velocity distribution approaches a fully developed profile). Experimental data confirmed this characteristic. Figure 3 indicates that, as anticipated, the u-v-p model can more accurately predict the location at which turbulent mixing is complete. It also predicted very little pressure variation with radial augmentor position as is known to be true experimentally.

2. **Test Case IIA - Medium Flow Rate/Zero Spacing**

   a. Velocity Profiles

   The results are presented in Figure 4 and, again, both computer predictions were very similar and agreed with

24

the limited experimental data at the augmentor exit plane.

b. Pressure Profiles

(1) $\psi-\omega$ Model. The pressure profile nearest
the centerline became more unrealistic for this higher flow
rate condition. The initial pressure drop was greatly exag-
gerated; however, the magnitude of the pressure rise was again
in good agreement with experiment. The pressure profile in
the quiescent flow region $(R = 0.38 R_a)$ did not agree with
the experimental curve. Both the pressure drop and rise in
the augmentor tube were underpredicted. In addition, the
minimum pressure point was predicted to occur about one engine
diameter downstream of the experimental minimum.

(2) u-v-p Model. The u-v-p model appears to
consistently underpredict the augmentor pressure drop and
rise. The slope of the pressure rise, however, was in reason-
able agreement with experiment. As discussed above, the pre-
dicted pressure profiles were determined by specifying the
inlet mass flow rates and uniform velocity profiles at the
engine exhaust and cell inlet. Table IV presents the effects
of changes in the specified flow rates on the predicted maxi-
mum pressure rise. Also shown in Table IV are the correspond-
ing values predicted using the one-dimensional equations for
conservation of mass, momemtum and energy. The latter calcu-
lations were made assuming perfect gases, coplanar engine exit
and augmentor inlet planes, no losses, and plug flow for both
inlets. The 1-D calculations do not correspond directly to
the 2-D calculations (no losses and plug flow of secondary air
at augmentor inlet). However, the predicted magnitudes of

TABLE IV

Effect of Input Variables on Predicted Pressure Profile

	CASE IIA (Test conditions)	CASE IIE 10% increase in $\dot{m}_e$	CASE IIF 9% decrease in $\dot{m}_a$
$\dot{m}_e (\frac{kg}{sec})$	0.690	0.759	0.690
$\dot{m}_a (\frac{kg}{sec})$	2.153	2.153	1.957
A.R.	3.12	2.84	2.84
$\Delta P_{maximum} \; n/m^2$ *	3714	6091	5089
$\Delta P_{maximum} \; n/m^2$ *	3628	4602	3795
$\Delta P_{maximum} \; n/m^2$ **	6200		

* calculated from one-dimensional equations; co-planar inlets with equal static pressures and with no losses

** experimental

26

Δp_{max} and the effects of changing flow rates should be similar. Table IV indicates that the 2-D and 1-D model predictions for the nominal case (II A) were in good agreement. However, the experimental Δp_{max} was considerably larger than predicted. Cases II E and II F show the predicted effects of 10% changes in the engine and secondary flow rates, respectively. The predicted 1-D effects were less than the 2-D effects but in the correct direction and sequence. It is seen that a net 10% error in the measured augmentation ratio ($\dot{m}_e$ from ASME orifice, $\dot{m}_t$ from augmentor exit pitot rake, and $\dot{m}_a = \dot{m}_t - \dot{m}_e$) could produce the differences between the experimental and 2-D model predictions. For example, an $\dot{m}_e$ larger by 3% and a total augmentor flow rate smaller by 3% (which are within the experimental accurary) would produce a decrease in augmentation ratio of approximately 8%. Thus, the differences between the predicted and measured pressure profiles may not be as large as depicted in Figure 4.

3. Test Case IIB - Medium Flow Rate/One Engine Diameter Spacing

a. Velocity Profiles

Experimental data were not available for this test condition. The predicted profiles are presented in Figure 5 and show that the two computer models predicted velocity profiles which were in close agreement. The primitive variable model, however, predicted a slightly greater initial jet spreading at the augmentor entrance and required a slightly longer duct length to obtain a fully developed profile.

27

b. Pressure Profiles

(1) $\psi-\omega$ Model. As for Case IIA, the centermost
pressure distribution greatly exaggerated the initial pressure
drop. In this case, the pressure rise also appeared to be
much too rapid in comparison to the $R = 0.38 R_a$ profile
and the u-v-p profiles. The profile in the quiescent flow
region was in reasonable agreement with the wall profile ob-
tained with the u-v-p model. The slopes of the pressure
rise and the minimum pressure predicted by both models were
nearly identical. The $\psi-\omega$ model, however, again predicted
the minimum pressure to occur somewhat farther downstream than
did the u-v-p model.

(2) u-v-p Model. For this case, the pressure
profile closest to the augmentor wall had a significantly
lower minimum pressure than the other profiles.

4. Test Case IIC - Medium Flow Rate/Two Engine
Diameter Spacing

a. Velocity Profiles

No empirical data were available for this test
condition. The computer predictions are presented in Figure 6.
As for Case IIB, the primitive variable model predicted greater
initial jet spreading. In this case, however, the $\psi-\omega$
velocity profiles became flat and the pressure profiles leveled
off considerably upstream of the u-v-p predicted profiles.

b. Pressure Profiles

(1) $\psi-\omega$ Model. The centermost pressure profile
was completely unrealistic. The quiescent region profile in-
dicated a larger pressure drop and rise and a minimum pressure

28

point farther downstream than the u-v-p model. In addition, the $\psi-\omega$ model profile leveled off much earlier.

(2) u-v-p Model. Again the minimum pressure was obtained for the profile closest to the augmentor wall and was located just inside the augmentor entrance. All the primitive variable curves indicate a more gentle augmentor pressure rise, leveling about midway down the augmentor tube.

5. Test Case III - High Flow Rate/Zero Spacing

a. Velocity Profiles

Substantially more experimental data were available for this test condition. In the experiment the nozzle was operated with a pressure ratio (p_{atm}/p_T) less than critical for one-dimensional isentropic flow. However, using the experimental nozzle flow rate and approximating the nozzle flow as one-dimensional and isentropic resulted in a nozzle exit Mach number of approximately 0.95. This condition was imposed on the models. As has been observed for the previous test cases, the velocity profiles for both models were quite similar (Figure 7) and in reasonably good agreement with experiment. However, the predicted profiles for both models tended to flatten a little too rapidly. The primitive variable model again predicted slightly more initial jet spreading at the augmentor inlet and less mixing down the augmentor tube than did the $\psi-\omega$ model. The experimental data more nearly agreed with the $\psi-\omega$ model at the augmentor inlet and with the u-v-p model downstream.

29

b. Pressure Profiles

(1) $\psi-\omega$ Model. Again the center pressure profile was completely unrealistic. The quiescent region pressure profile underpredicted the augmentor pressure drop and rise. The minimum pressure position was substantially displaced down the augmentor tube and the slope of the pressure rise did not agree with experiment.

(2) u-v-p Model. All three u-v-p pressure profiles were quite similar. They underpredicted both the augmentor pressure drop and rise. The slope of the pressure rise was in good agreement with experimental data within the first half of the augmentor tube. The predicted pressure profiles from both the $\psi-\omega$ and u-v-p models leveled off before the experimental curves.

C. COMPUTATIONAL ACCURACY AND REQUIRED COMPUTER TIME

The utility of any computer program using numerical methods is reflected by the amount of CPU time required and the ease of arriving at converged solutions. Table V compares the percentage change in variable magnitude on successive iterations and the required CPU time.

A considerable savings in CPU time was obtained using the line-by-line iterative procedure of the primitive variable model in lieu of the point-by-point (Gauss-Seidel) method employed in the $\psi-\omega$ model.

At low flow rates, the convergence was quite similar for both models. However, at higher flow rates the u-v-p model had better convergence in less time.

TABLE V. COMPARISONS OF CPU TIME AND $(\Delta\phi/\phi)\cdot100$ FOR LAST CALCULATION

	CPU TIME (MIN)	VORTICITY	STREAM FUNCTION	AXIAL VELOCITY	PRESSURE MINUS REF PRESSURE	TURBULENCE KINETIC ENERGY	DISSIPATION RATE
CASE I mass flow = .45 kg/sec AR = 3.26 spacing = 0	138.5 / 21.6	.15	.041 / -	- / 0 / 1.17	- / 0 / .24	.19 / 0 / .11	.0004 / .15 / .15
CASE IIA mass flow = .69 kg/sec AR = 3.12 spacing = 0	139.2 / 29.1	.20	.08 / -	- / .12 / .64	- / .68 / .68	.27 / .36 / .36	.003 / 0 / .03
CASE IIB mass flow = .69 kg/sec AR = 3.12 spacing = 1 eng dia	145.4 / 32.9	.79	.18 / -	- / .12 / 0	- / 0 / .28	.32 / 0 / 0	.0003 / 0 / 0
CASE IIC mass flow = .69 kg/sec AR = 3.12 spacing = 2 eng dia	159.3 / 20.8	3.1	.44 / -	- / 0 / 0	- / .63 / .63	3.14 / 0 / .46	3.5 / .16 / .16
CASE III mass flow = .99 kg/sec AR = 2.9 spacing = 0	148.7 / 22.8	.43	.098 / -	- / 0 / .55	- / .15 / .15	.29 / 0 / .07	.001 / 0 / .08

Legend:
- ψ-ω model - worst case in field
- U-V-P model - worst case in augmentor
- U-V-P model - worst case in field

31

D. COMPUTER RELATED PROBLEMS

Both models required that the proper relaxation parameters be selected in order to obtain convergence. The lack of any procedure for selecting the proper relaxation values makes this process quite time consuming. Previous research using the $\psi-\omega$ model facilitated the selection of these parameters for that model. It was found that the u-v-p model was quite sensitive to the calculated "pressure corrections". Obtaining the correct underrelaxation value for pressure proved to be the key in arriving at a converged solution for the primitive variable model.

The line-by-line iterative procedure used in the u-v-p model was, as expected, quite good in propagating disturbances downstream when sweeping from left to right. A downstream disturbance is propagated upstream by successive sweeps through the entire field. This fact, at least for a geometry incorporating a sudden contraction, made the convergence dependent on the number of traverses on each radial line. An excessive number of traverses would cause divergence. The number of traverses on each line was controlled in two ways. After each traverse, residual factors were calculated for each variable and the largest residual factor was compared to a pre-set value. If the largest residual was less than the pre-set value, the program advanced to the next radial line. The program would also advance when a pre-set maximum number of traverses had been completed on any radial line. To aid convergence, only a few traverses on each line were allowed

until several sweeps through the field had allowed the presence of the contraction wall to be "felt" upstream. The number of traverses on a line was then increased. It was additionally found that when working with coaxial flows with radically different inlet velocities, the normalizing factors (which were based on average inlet conditions and used to calculate the residual values on each line) resulted in excessive traverses being made in regions of high flow velocity. Repeated calculations on radial lines which had already converged often caused divergence. Adjusting the normalizing factors downstream of the engine exit alleviated this problem.

The primitive variable model demonstrated some convergence difficulty in the recirculation region adjacent to the sudden contraction. This problem could have resulted from the relatively large normalizing factors used in this local region of low velocity or, as suggested by Launder and Spalding [12], it could have possibly been due to the inadequacy of the empirical constants (Table I) in the K-ε model for the flow in this quiescent zone.

As with any finite difference numerical solution, grid spacing was found to be critical. To aid convergence, the grid spacing was decreased in all regions where large property gradients were expected. Gosman, et al [1] recommended that for the ψ-ω model, successive spacing should not increase by more than about a factor of 1.5. This restriction was also employed for the primitive variable model. A 30 by 30 grid system was utilized for the primitive variable model,

whereas a 43 by 40 grid was required for the ψ-ω model.

E. SUMMARY OF RESULTS - PRESSURE AND VELOCITY DISTRIBUTIONS

In most cases the predicted velocity profiles for both the ψ-ω and u-v-p computer models agreed with each other and with the available experimental data. The u-v-p model predicted more initial jet spreading at the augmentor inlet, especially in those cases where the engine exit plane was not flush with augmentor inlet. Both models predicted that a flat velocity profile was obtained where the pressure profile leveled off. For the one case in which experimental data were available over the entire legnth of the augmentor tube, the predicted velocity profiles seemed to flatten slightly faster than the experimental data.

In general, the ψ-ω model demonstrated poor pressure prediction capability. For low flow rates the pressure rise on the wall from minimum to maximum was accurately predicted for a pressure profile calculated near the axis of symmetry. For higher flow rates the centermost predictions became unrealistic although converged solutions were obtained for all primary variables. For the predicted pressure profiles along axial lines that were in the quiescent flow region, the ψ-ω model characteristically unpredicted the pressure drop and rise along the augmentor wall. The minimum predicted pressure location was typically somewhat downstream of its experimentally determined position.

The primitive variable model predicted little radial pressure variations except near the engine exit plane. It seemed

34

to accurately locate the minimum pressure position and to predict the rapid pressure drop at the augmentor entrance. It consistently underpredicted the pressure drop and rise in the augmentor but tended to accurately predict the slopes of the rising pressure profiles. However, as discussed above, reasonably expected experimental errors could account for these differences. Application of the $K-\epsilon$ turbulence model with fixed parameters (C_D, C_1, C_2, σ_ϵ, σ_K) to the test cell flow conditions may also be a reason for the lack of quantitative accuracy in the predicted pressure profiles. Further experimental data (for example, turbulence intensity measurements) are needed to further validate the model.

The primitive variable model appears to reasonably predict the flow field up to sonic engine exhaust conditions. These predictions include realistic pressure distributions and require substantially less computer time and fewer grid lines than the $\psi-\omega$ model.

F. RESULTS AND DISCUSSION - NOISE CONSIDERATIONS

Computer model predictions for the velocity, turbulence kinetic energy and pressure distributions are presented in Figures 8, 9 and 10. The predictions were for the two inches diameter nozzle at high mass flow rate (Run 1, Table VI). The four curves on each figure are for different radial positions; jet centerline, just inside the jet exhaust radius; just outside the jet exhaust radius, and near the augmentor wall.

Run No.	Nozzle Exit Diameter (in.)	ENGINE			"Orifice" Peak frequency, V/2d (HZ)	AUGMENTOR TUBE		SECONDARY AIR	
		$T(^{\circ}F)$	$\dot{M}_E \left(\frac{lb_m}{sec}\right)$	V_E (FPS)		$\dot{M}_A \left(\frac{lb_m}{sec}\right)$	V_A (FPS)	$\dot{M}_{SA} \left(\frac{lb_m}{sec}\right)$	V_{SA} (FPS)
1	2	88.8	1.44	866	2597	4.78	114.6	3.34	94.2
2	2	90.5	.50	297	892	1.95	46.9	1.46	41.2
3	3.5	93.0	1.97	386	661	2.93	70.3	.96	27.1

TABLE VI. SUMMARY OF TEST DATA FOR NOISE EXPERIMENTS

Noise intensities for selected frequency ranges as a function of augmentor tube position are displayed in Figures 11, 12 and 13.

Figures 14 through 16 and Table VII compare the basic test results to data obtained at one transducer port after the microphone was insulated and the "building wall" location was changed.

Figure 11 presents the data for the small nozzle with a high subsonic exhaust velocity $(M_e \approx 0.75)$. The highest frequencies were greater than peak values expected from orifice data $(V/2d)$ but were apparently generated near the nozzle exit as expected. If the high frequencies generated near the nozzle exit were radiated at 45° to the axis, the corresponding peak intensities would occur between two and five jet diameters downstream. The lowest frequencies peaked in intensity at approximately 20 jet diameters downstream in general agreement with data from free jets emitted from orifice plates [14]. The intensity increased as the frequency decreased.

Figure 12 presents the data for the small nozzle with a very low exit velocity $(M_e \approx 0.25)$. The data had similar characteristics to that for the high exit velocity: (1) the intensity increased with decreasing frequency, (2) the peak frequencies were greater than $V/2d$ and (3) the lowest frequencies peaked in intensity at approximately 20 jet diameters downstream. In this case, however, the highest frequencies peaked in intensity further downstream.

Run No.	Nozzle Exit Diameter (in.)	$T_E(^\circ F)$	$\dot{M}_E(\frac{lb_m}{sec})$	V_E (FPS)
1	2	88.8	1.44	866
1a		91.0	1.52	914
2	2	90.5	.50	297
2a		84.9	.53	316
3	3.5	93.0	1.97	386
3a		95.5	1.97	385

TABLE VII. TEST DATA FOR MODIFIED NOISE EXPERIMENTS

Figure 13 presents data for the larger nozzle with low exit velocity. The data were similar to Figure 12 except that the intensity did not vary as consistently with frequency range. The peak intensity did occur for the lowest frequency range and occurred at approximately 10 jet diameters downstream. This peak intensity was at the same augmentor position as for the smaller nozzle at low exit velocity (Figure 12).

The possibility existed that some of the sound recorded was either being reflected from or was due to the physical resonance of surrounding structures. However, the data presented in Figures 14 and through 16 indicate that these effects were not large.

The computer predictions made for the distributions of axial velocity, turbulence kinetic energy and pressure (Figures 8, 9 and 10) were for the test conditions/results presented in Figure 11. (RUN No. 1, Table VI.)

The peak intensities for the lower frequency sound noted above occurred approximately at the predicted location within the augmentor tube at which, (1) turbulent mixing became essentially complete, (2) pressure reached a maximum, and (3) the axial velocity profile became fairly constant. The decay in the predicted turbulence kinetic energy (Figure 9) followed closely the rise in noise amplitude for the two lower frequency ranges (Figure 11).

The data were much too limited to draw any general conclusions. However, the results indicate that the maximum sound intensities occur within the augmentor tube in the

region where jet mixing is nearing completion. If this observation is correct, it would enable the computer model to be used for full scale test cells to predict the best placement of sound suppressors/jet breakup devices for varying test cell geometries and engine operating conditions.

V. CONCLUSIONS

The primitive variable computer model for the turbojet test cell appears to reasonably predict the flow field for engine exhaust conditions up to the sonic condition. The conclusion is based upon subscale test cell measurements of velocity and pressure distributions. To further validate the model, comparisons should be made with full scale test cell data. In addition, turbulence intensity distributions measured within the subscale test cell would provide valuable new data for additional model validation.

VI. REFERENCES

1. Gosman, A. D., and others, <u>Heat and Mass Transfer in Recirculating Flows</u>, Academic Press, 1969.

2. Hayes, J. D. and Netzer, D. W., "An Investigation of the Flow in Turbojet Test Cells and Augmentors," Naval Postgraduate School Report Number NPS-57-Nt-75101, Monterey, CA, October 1975.

3. Mongia, H. C. and Reynolds, R. S., "Combustor Design Criteria Validation Volume III," AIRESEARCH Manufacturing Company of Arizona Report Number USARTL-TR-78-55c, February 1979.

4. Croft, D. R. and Lilley, D. G., "Finite-Difference Performance Analysis of Jet Pumps," AIAA Journal, Volume 14, No. 10, p. 1347-1378, October 1976.

5. Netzer, D. W., "Modeling Solid-Fuel Ramjet Combustion," Journal of Spacecraft and Rockets, Volume 14, Report No. 12, p. 762-766, December 1977.

6. Walters, J. J. and Netzer, D. W., "A Validation of Mathematical Models for Turbojet Test Cells," Naval Postgraduate School Report Number NPS-67-78-002, Monterey, CA, June 1978.

7. Speakman, G. C., Hayes, J. D. and Netzer, D. W., "Internal Aerodynamics of Turbojet Test Cells," Naval Postgraduate School Report Number NPS-67Nt-76121, Monterey, CA, December 1976.

8. Pun, W. M. and Spalding, D. B., "A General Computer Program for Two-Dimensional Elliptic Flows," Imperial College of Science and Technology, Report No. HTS/76/2, August 1977.

9. Kays, W. M., <u>Convective Heat and Mass Transfer</u>, McGraw-Hill, 1966.

10. Launder, B. E. and Spalding, D. B., "The Numerical Computation of Turbulent Flows," Computer Methods in Applied Mechanics and Engineering, p. 269-289, August 1973.

11. Jones, W. P. and Launder, B. E., "The Prediction of Laminarization with a Two-Equation Model of Turbulence," INT. J. Heat Mass, Transfer, Volume 15, p. 68-87, 1972.

12. Launder, B. E. and Spalding, D. B., <u>Lectures in Mathematical Models of Turbulence</u>, Academic Press, 2nd edition, 1976.

13. Lighthill, J. J., "General Theory on Sound Generated Aerodynamically," PROC. ROY. SOC. (LONDON), A211 p. 564-587, 1972.

14. Lighthill, J. J., "Turbulence as a Source of Sound," PROC. ROY. SOC. (LONDON), p. 1-32, 1954.

15. Hewlett, H. W., Hickey, P. J. and Netzer, D. W., "A Subscale Turbojet Test Cell for Design Evaluations and Analytical Model Validation," Naval Postgraduate School Report Number NPS-67-Nt-77091, Monterey, CA, September 1977.
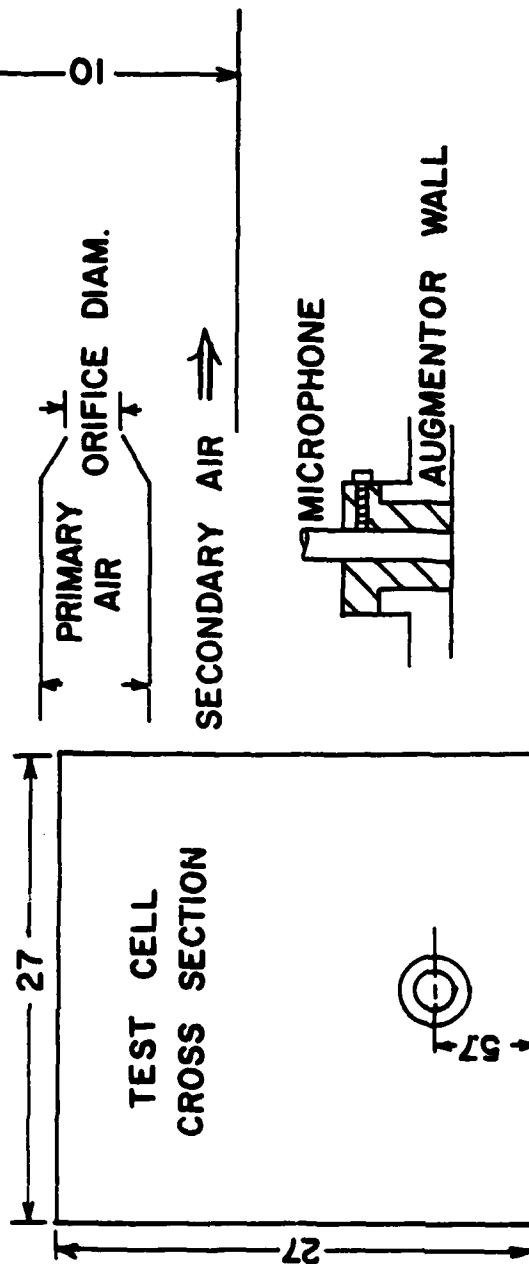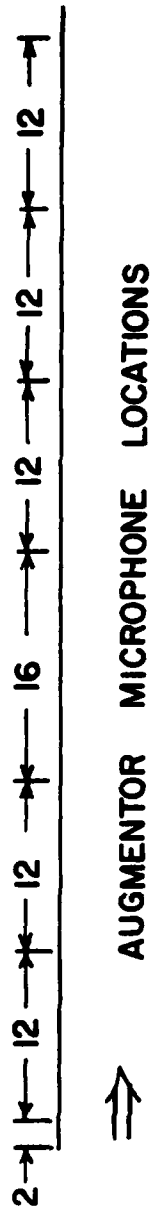
WALLS

$u = 0$
$v = 0$

$\frac{\partial h}{\partial x}$ or $\frac{\partial \tilde{h}}{\partial r} = 0$

$K_p = K_p(\tau_w)$
$\varepsilon_p = \varepsilon_p(k_p, \delta)$

EXIT

$v = 0$

$\frac{\partial \phi}{\partial x} = 0$

AUGMENTOR

2.44 m

0.1 m

SECONDARY FLOW

SPACING

0.3 m

.387 m

ENGINE FLOW

.025 m

CENTER LINE

$v = 0$

$\frac{\partial \phi}{\partial r} = 0$

INLETS

$u = u_{in}$
$v = 0$
$\tilde{h} = h_{in}$
$k = .005\ u_{in}^2$
$\varepsilon = .09k^{3/2}/.03r$

SPACING

CASE I	0
CASE IIA	0
B	1 ENG DIA
C	2 ENG DIA
CASE III	0

FIGURE 1. TURBOJET TEST CELL GEOMETRY AND BOUNDARY CONDITIONS

FIGURE 2. TURBOJET TEST CELL DIMENSIONS FOR NOISE MEASUREMENTS
(DIMENSIONS IN INCHES)

45
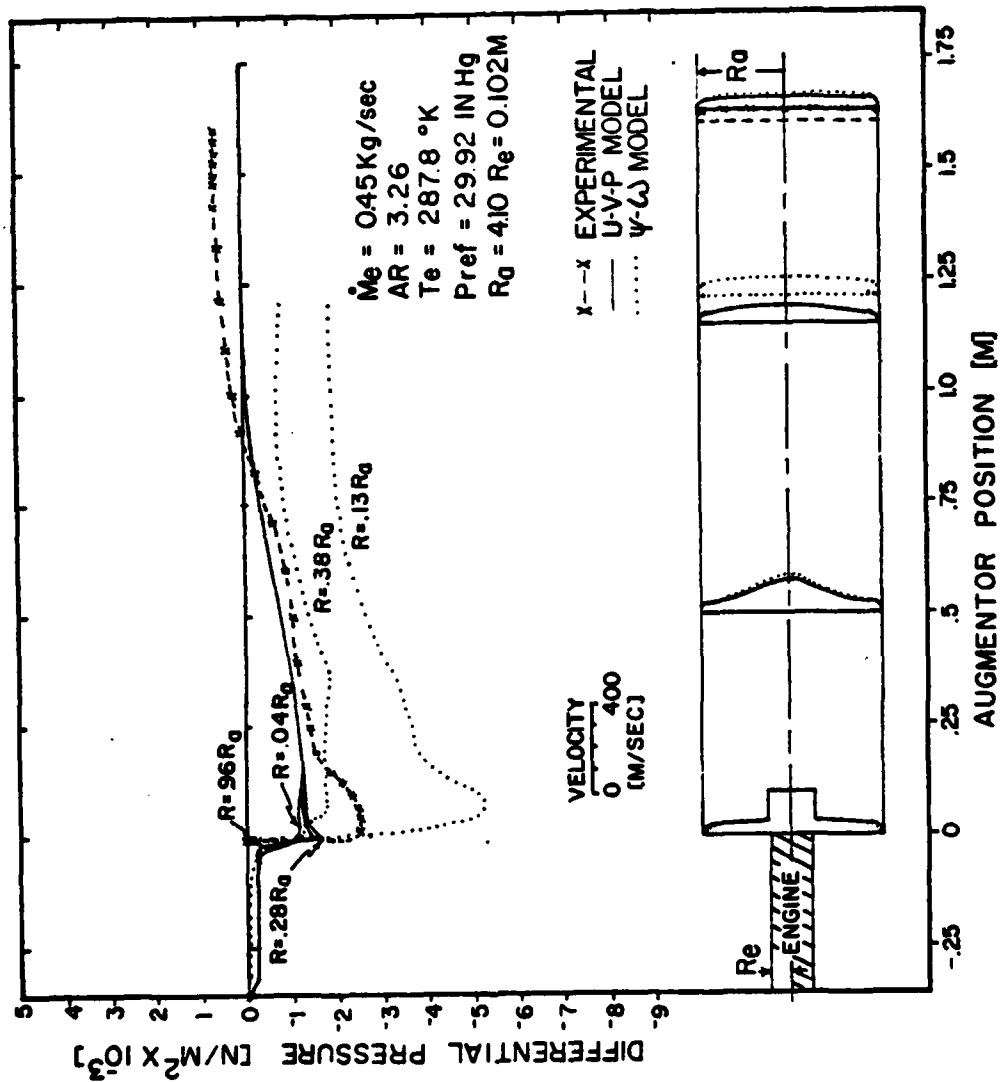
FIGURE 3. AUGMENTOR PRESSURE AND VELOCITY PROFILES FOR STRAIGHT PIPE INLET AND ZERO ENGINE-AUGMENTOR SPACING, $\dot{m}_e = 0.45$ kg/sec

46
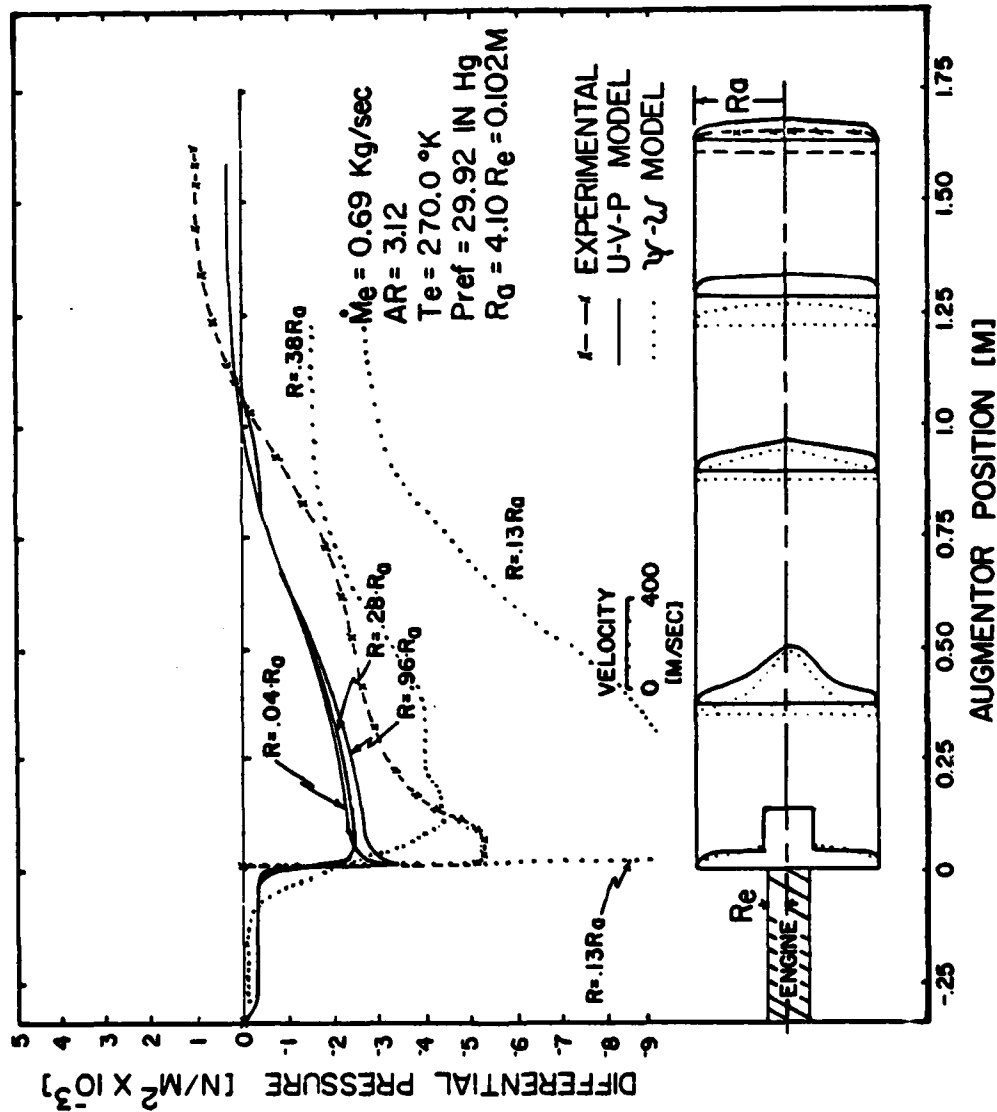
FIGURE 4. AUGMENTOR PRESSURE AND VELOCITY PROFILES FOR STRAIGHT PIPE INLET AND ZERO ENGINE-AUGMENTOR SPACING, $\dot{m}_e$ = 0.69 kg/sec

47

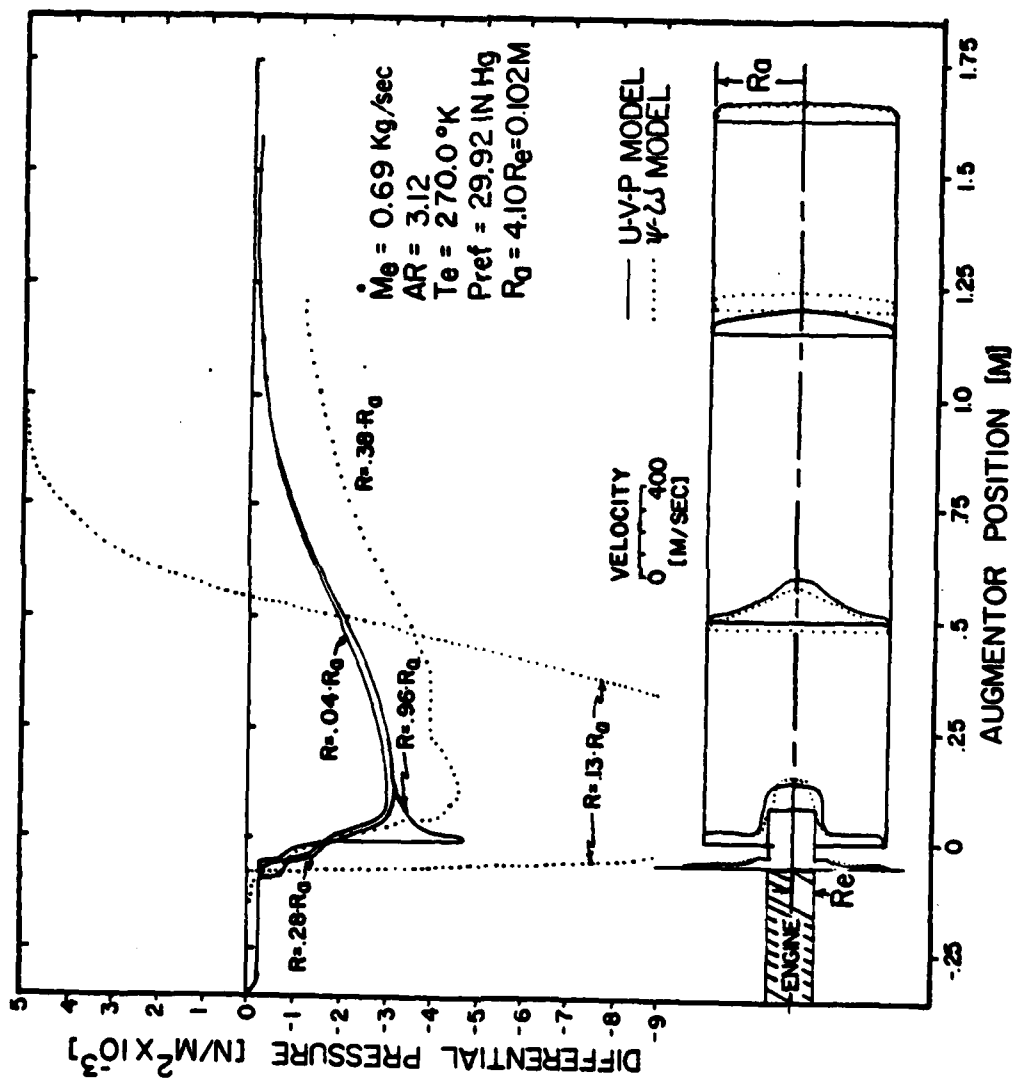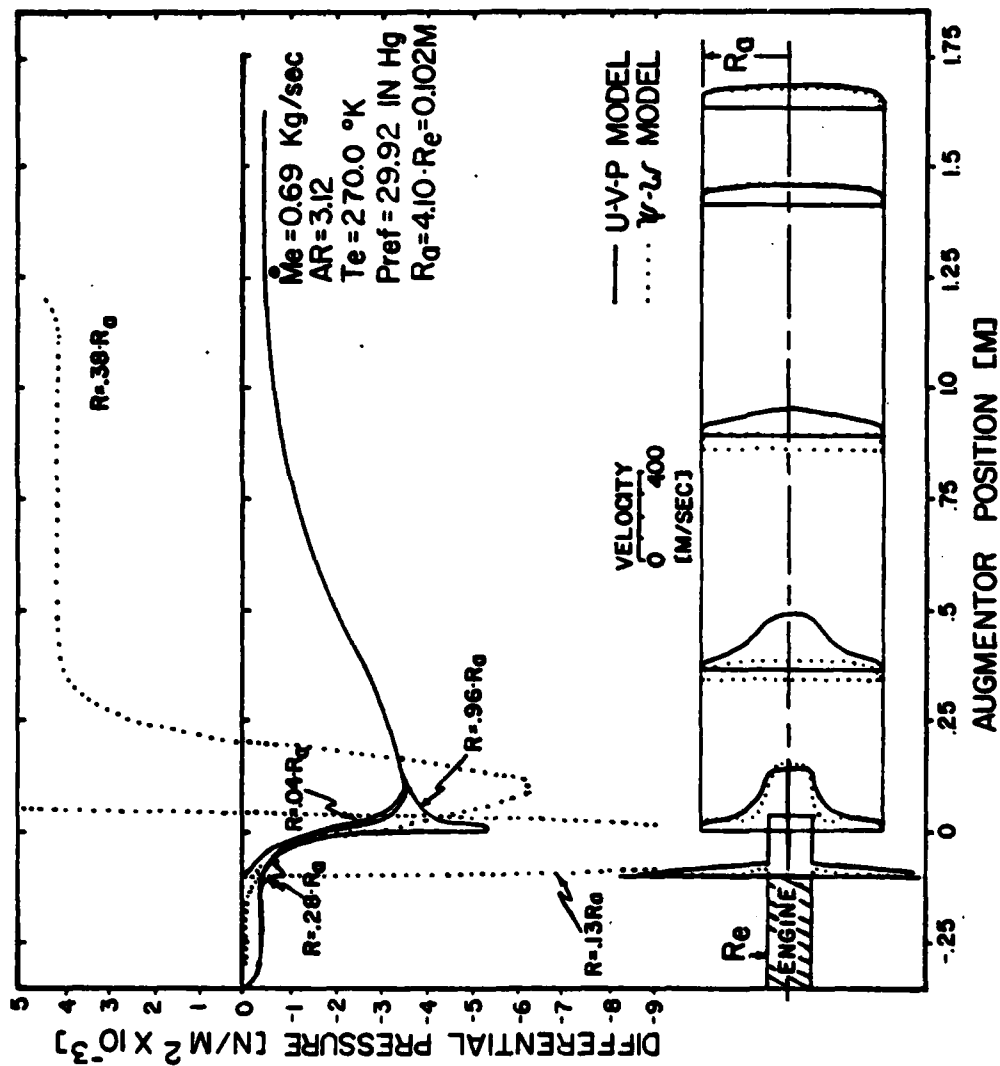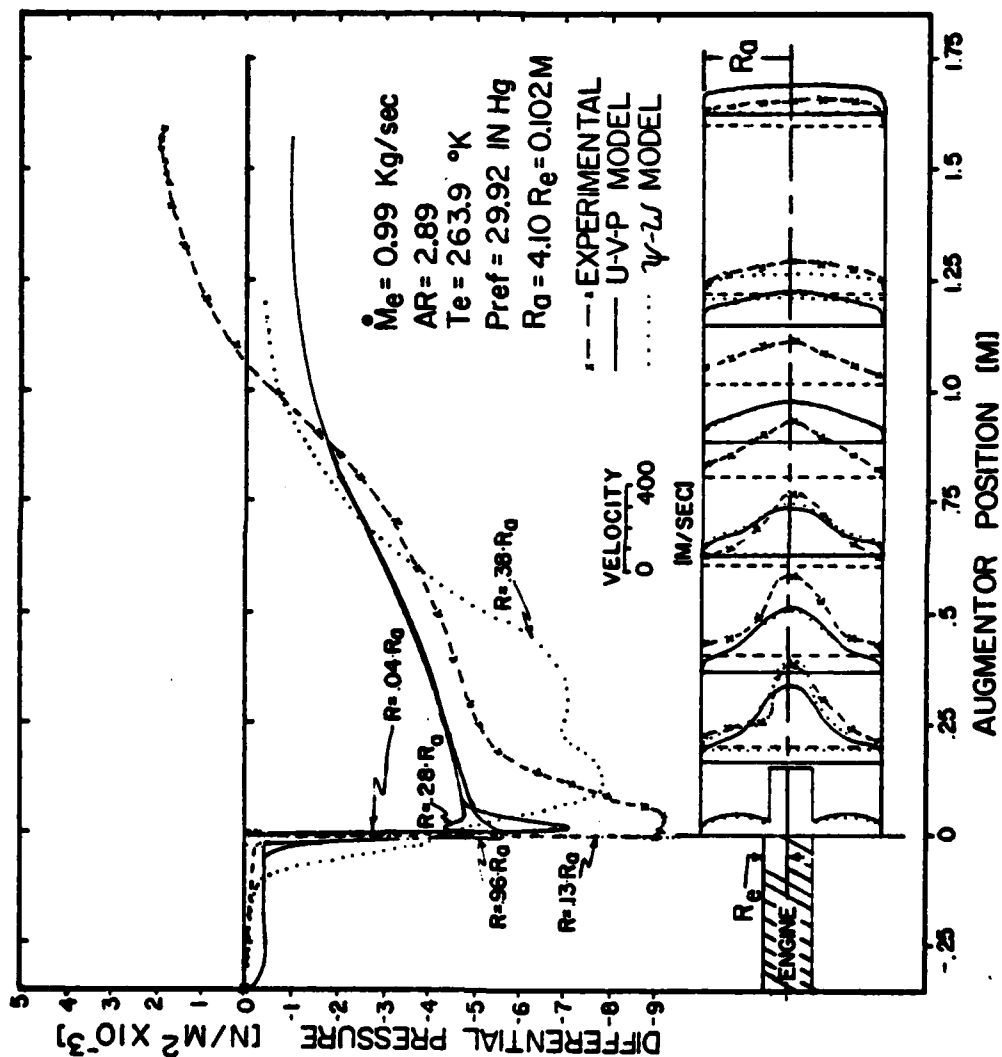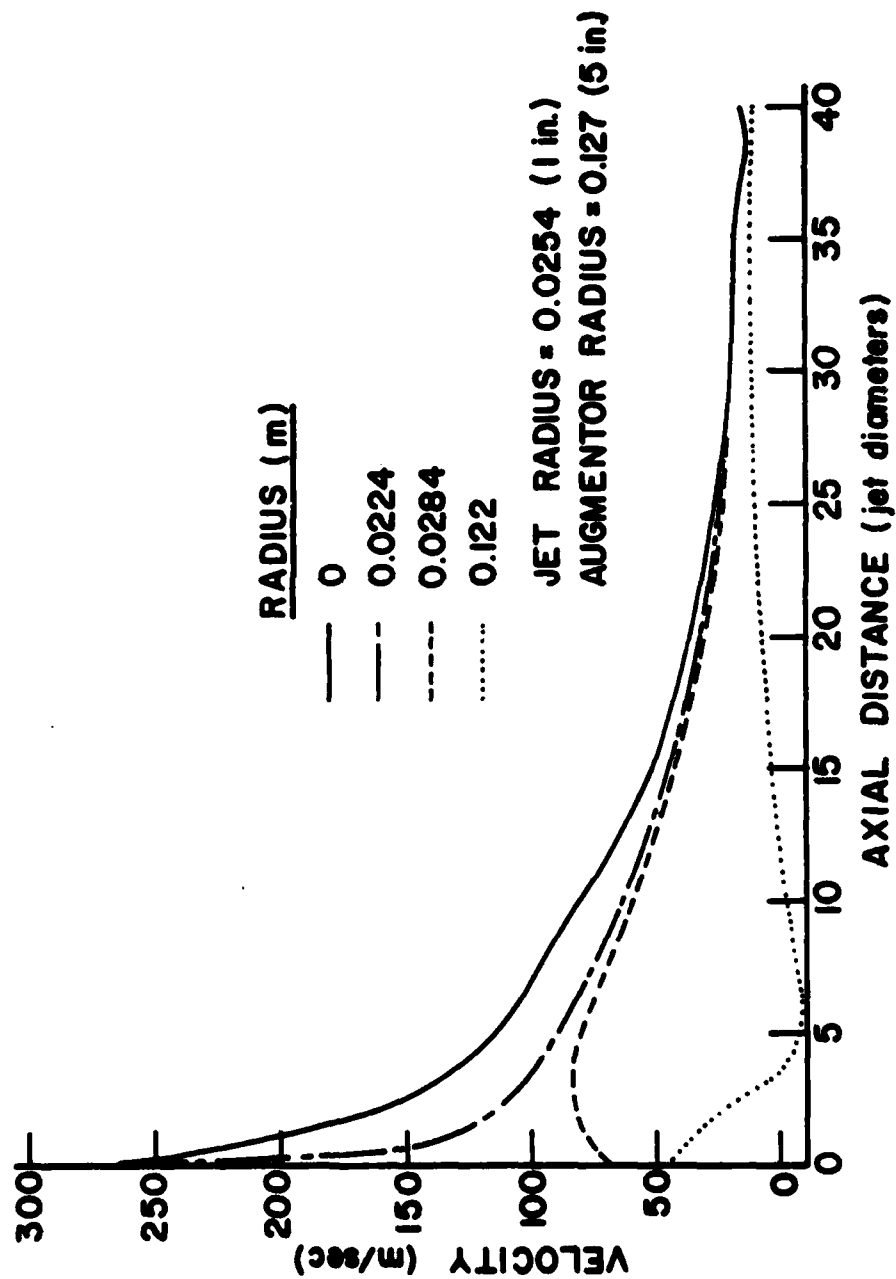FIGURE 5. AUGMENTOR PRESSURE AND VELOCITY PROFILES FOR STRAIGHT PIPE INLET AND ONE DIAMETER ENGINE-AUGMENTOR SPACING, $\dot{m}_e = 0.69$ kg/sec

48

FIGURE 6. AUGMENTOR PRESSURE AND VELOCITY PROFILES FOR STRAIGHT PIPE INLET AND TWO DIAMETER ENGINE-AUGMENTOR SPACING, $\dot{m}_e = 0.69$ kg/sec

FIGURE 7. AUGMENTOR PRESSURE AND VELOCITY PROFILES FOR STRAIGHT PIPE INLET AND ZERO ENGINE-AUGMENTOR SPACING, $\dot{m}_e$ = 0.99 kg/sec
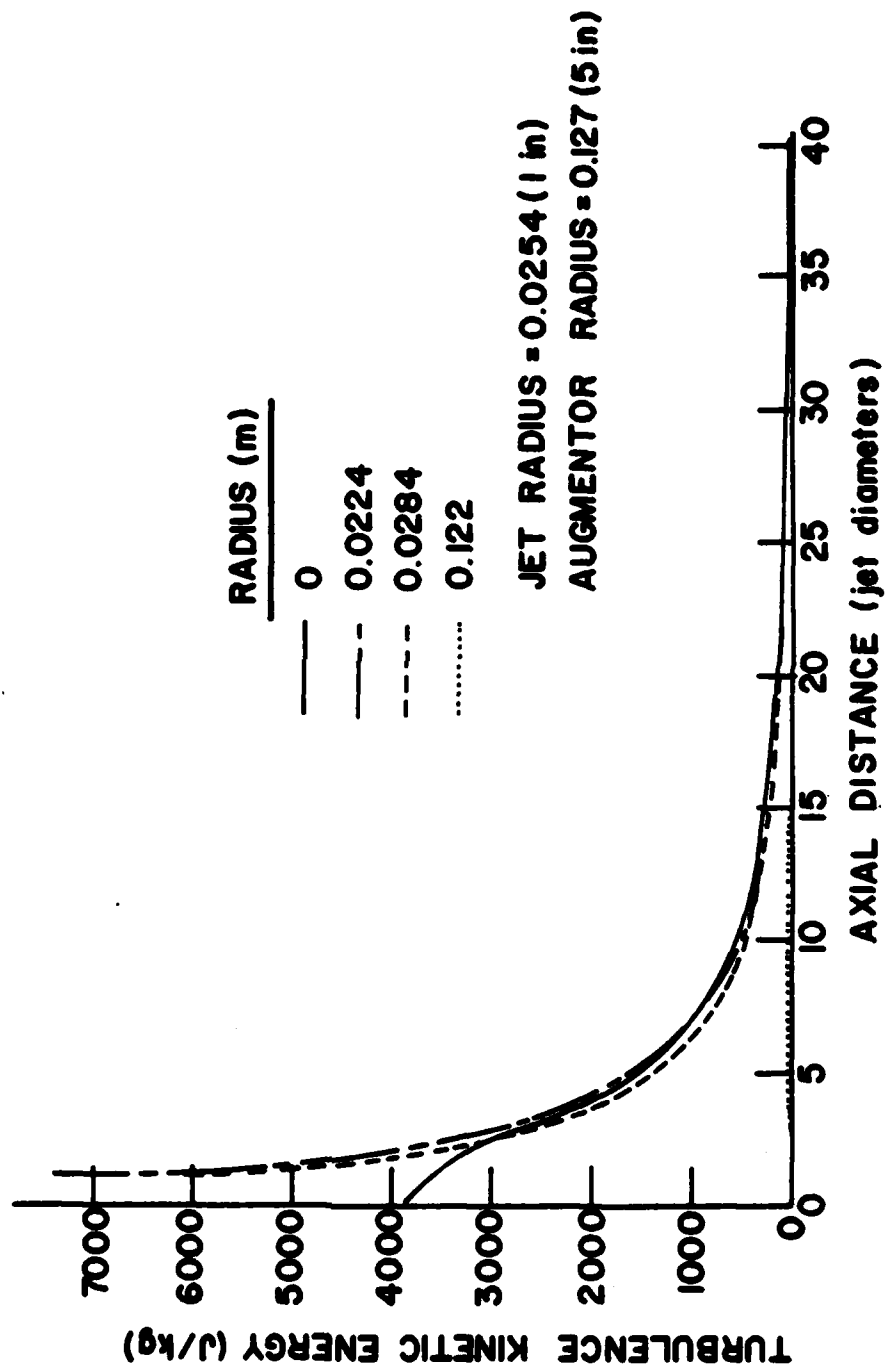
FIGURE 8. PREDICTED VELOCITY PROFILES

51

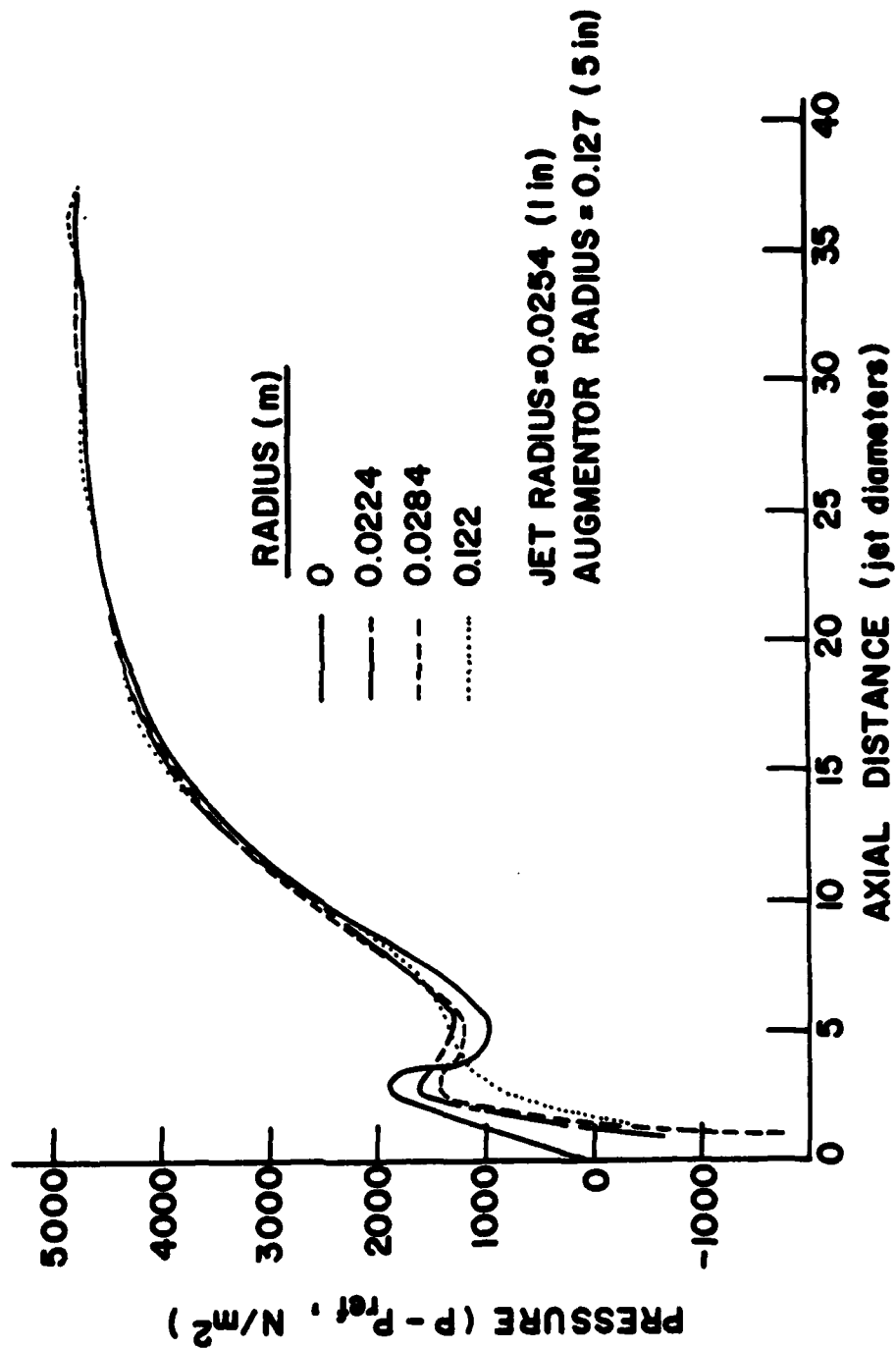FIGURE 9. PREDICTED TURBULENCE KINETIC ENERGY PROFILES
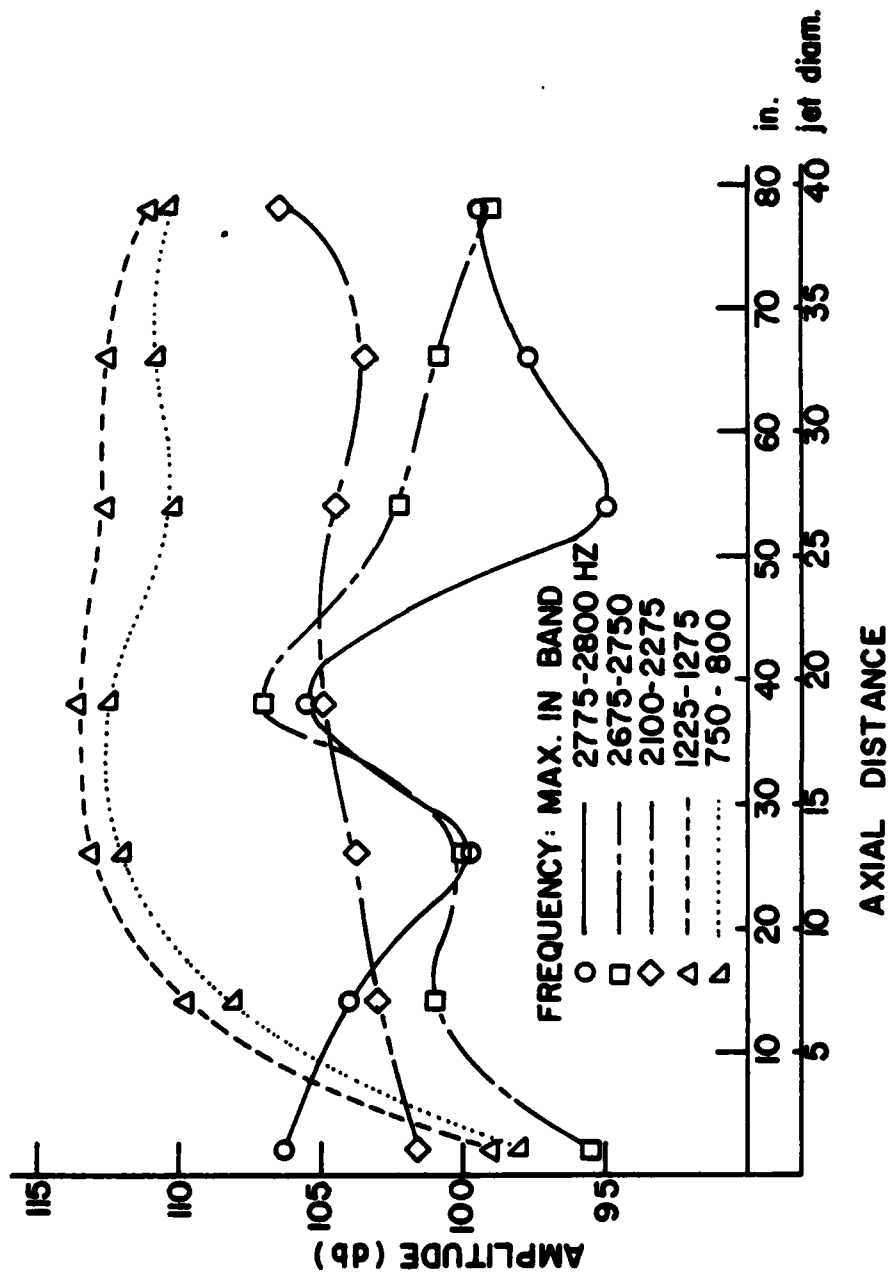
FIGURE 10. PREDICTED PRESSURE DISTRIBUTIONS

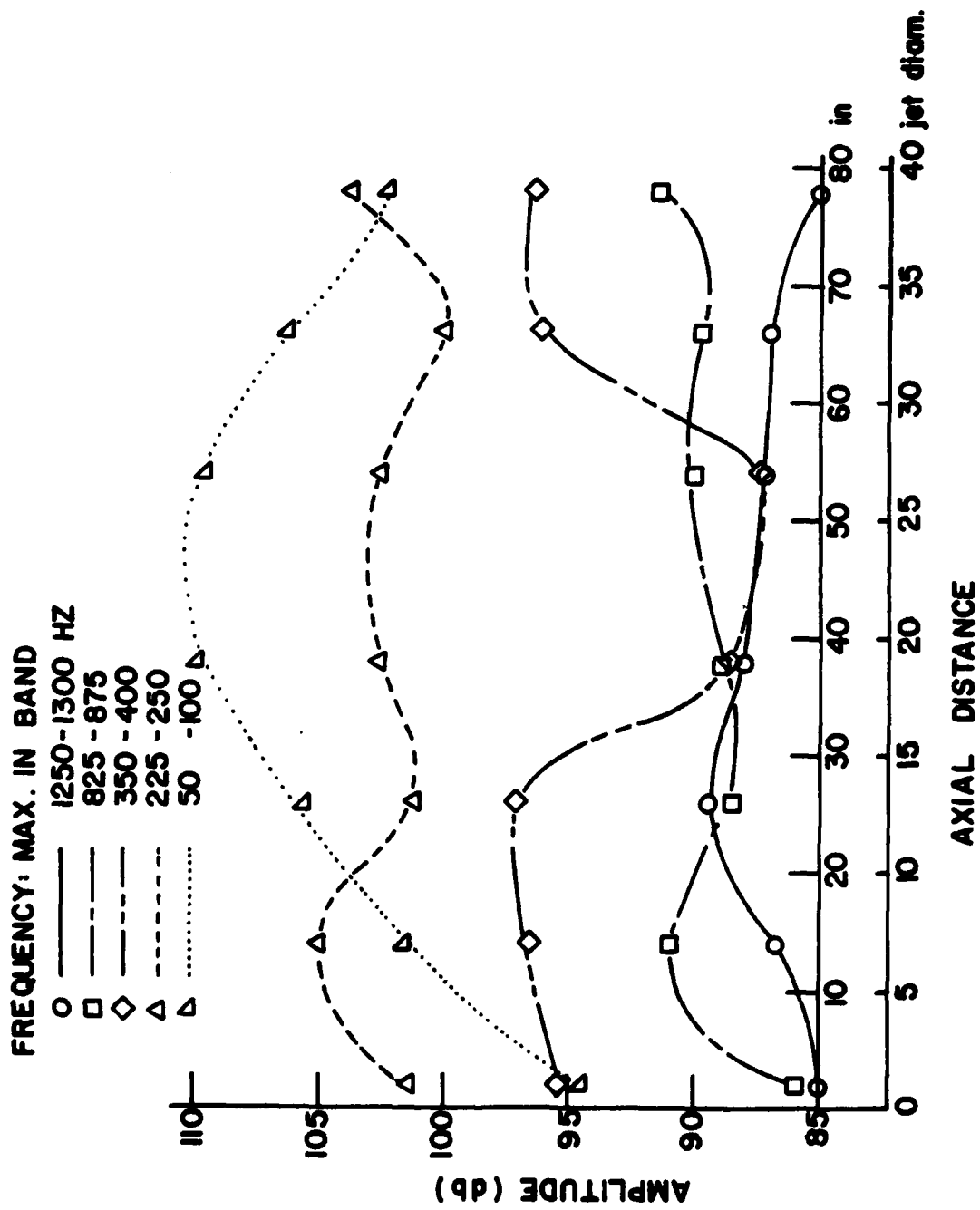FIGURE 11. NOISE INTENSITY VS. AUGMENTOR TUBE POSITION, RUN NO. 1

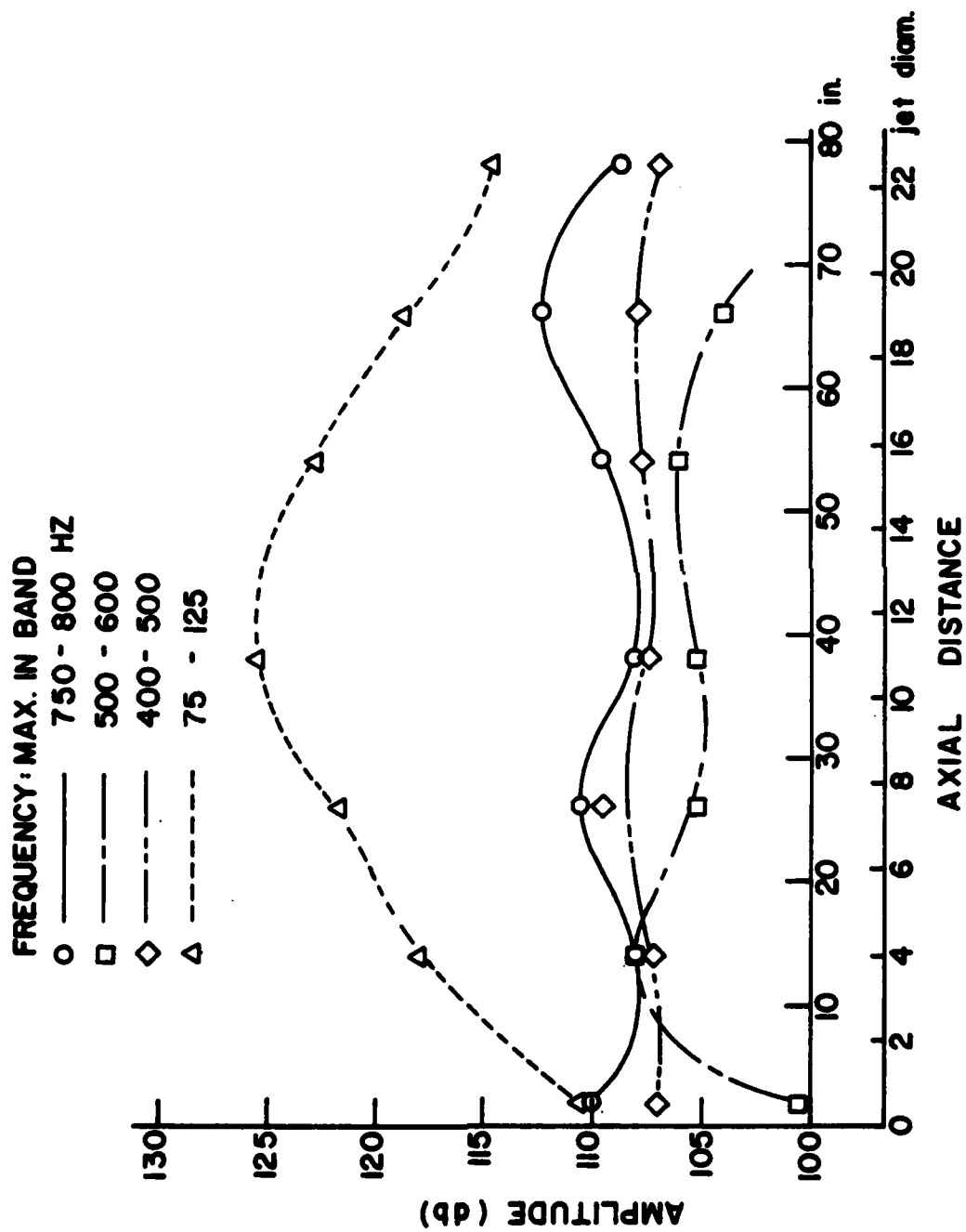FIGURE 12. NOISE INTENSITY VS. AUGMENTOR TUBE POSITION, RUN NO. 2

55

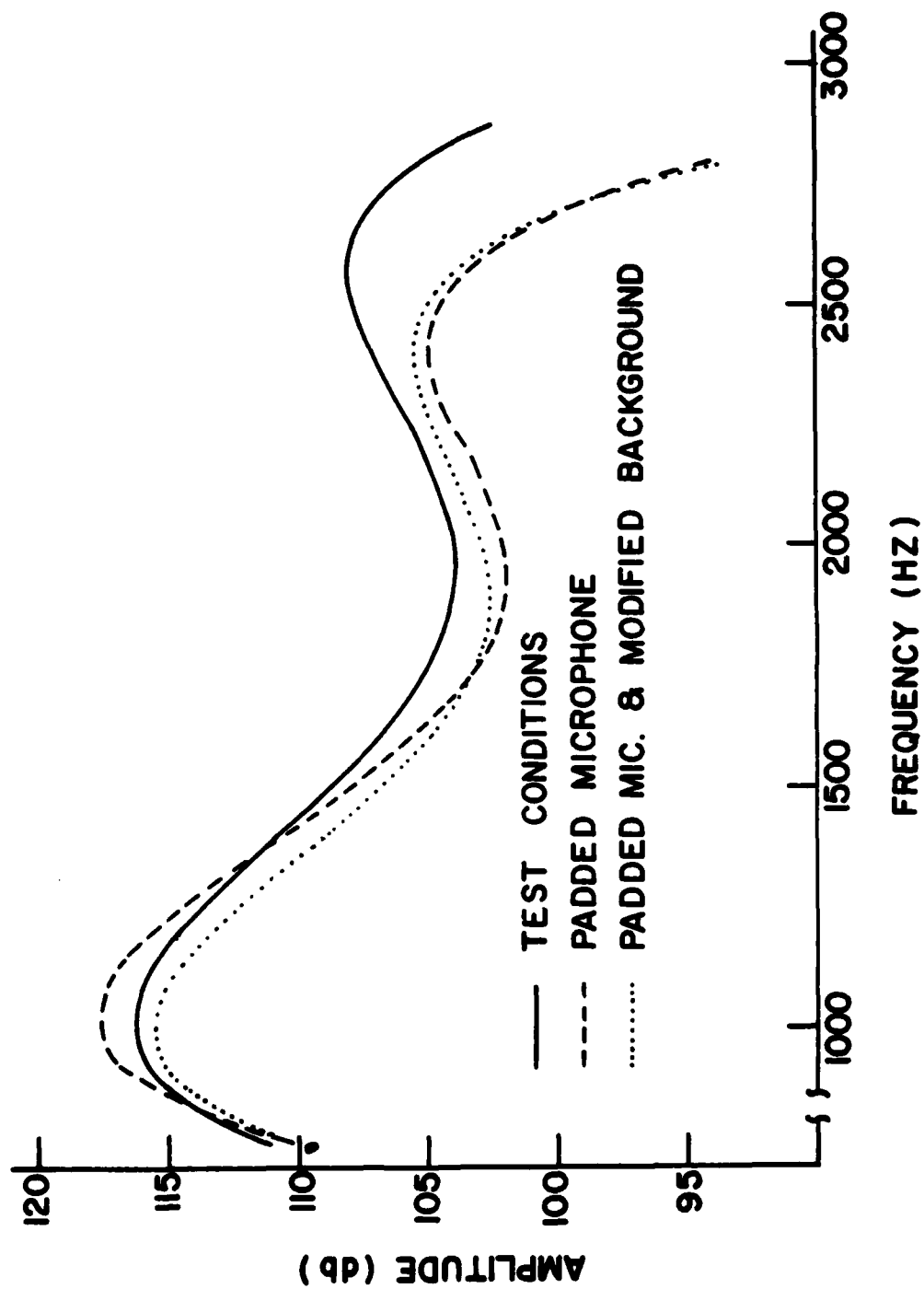FIGURE 13. NOISE INTENSITY VS. AUGMENTOR TUBE POSITION, RUN NO. 3

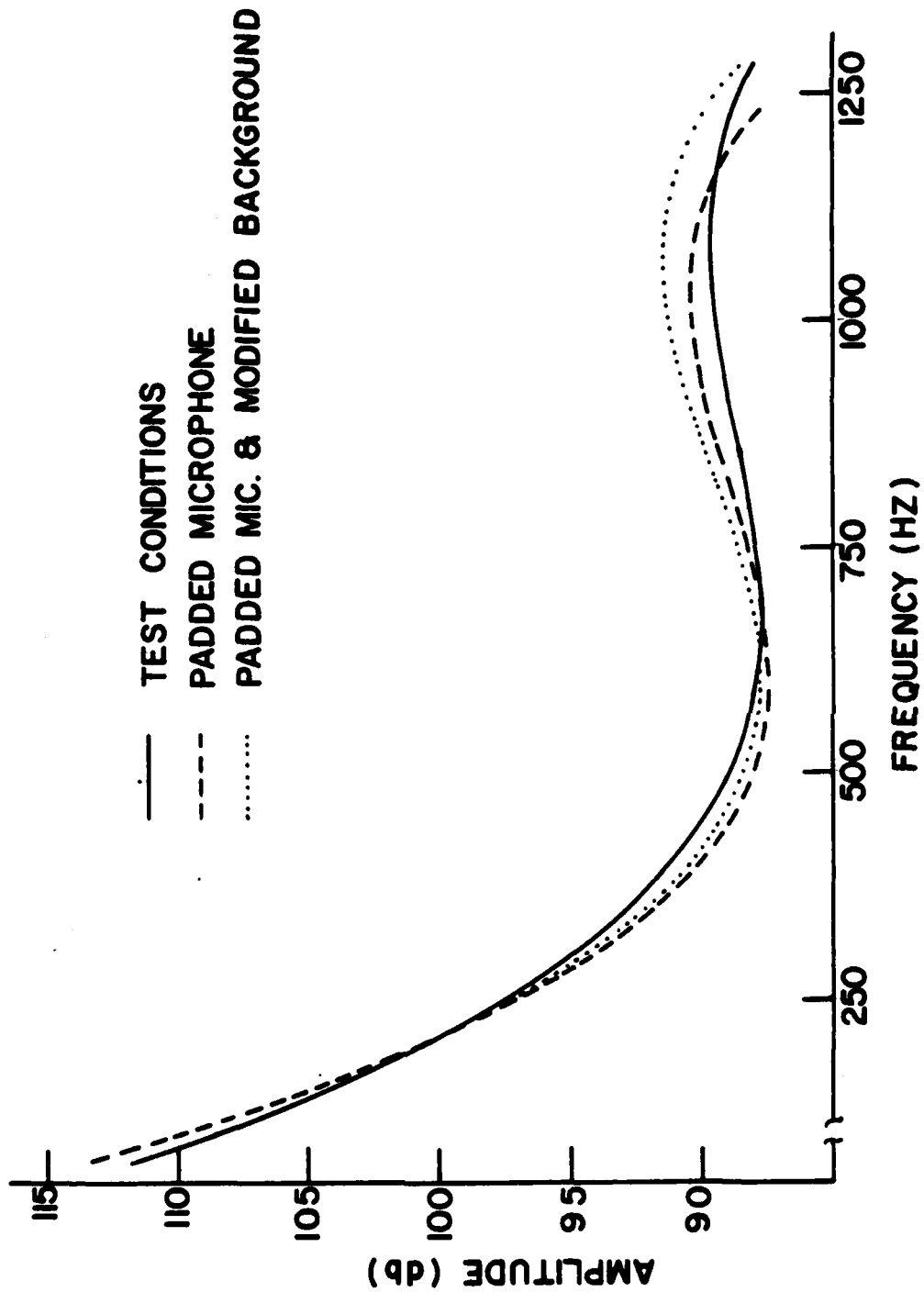FIGURE 14. NOISE INTENSITY VS. FREQUENCY, RUNS 1 AND 1a

57

FIGURE 15. NOISE INTENSITY VS. FREQUENCY, RUNS 2 AND 2a

58

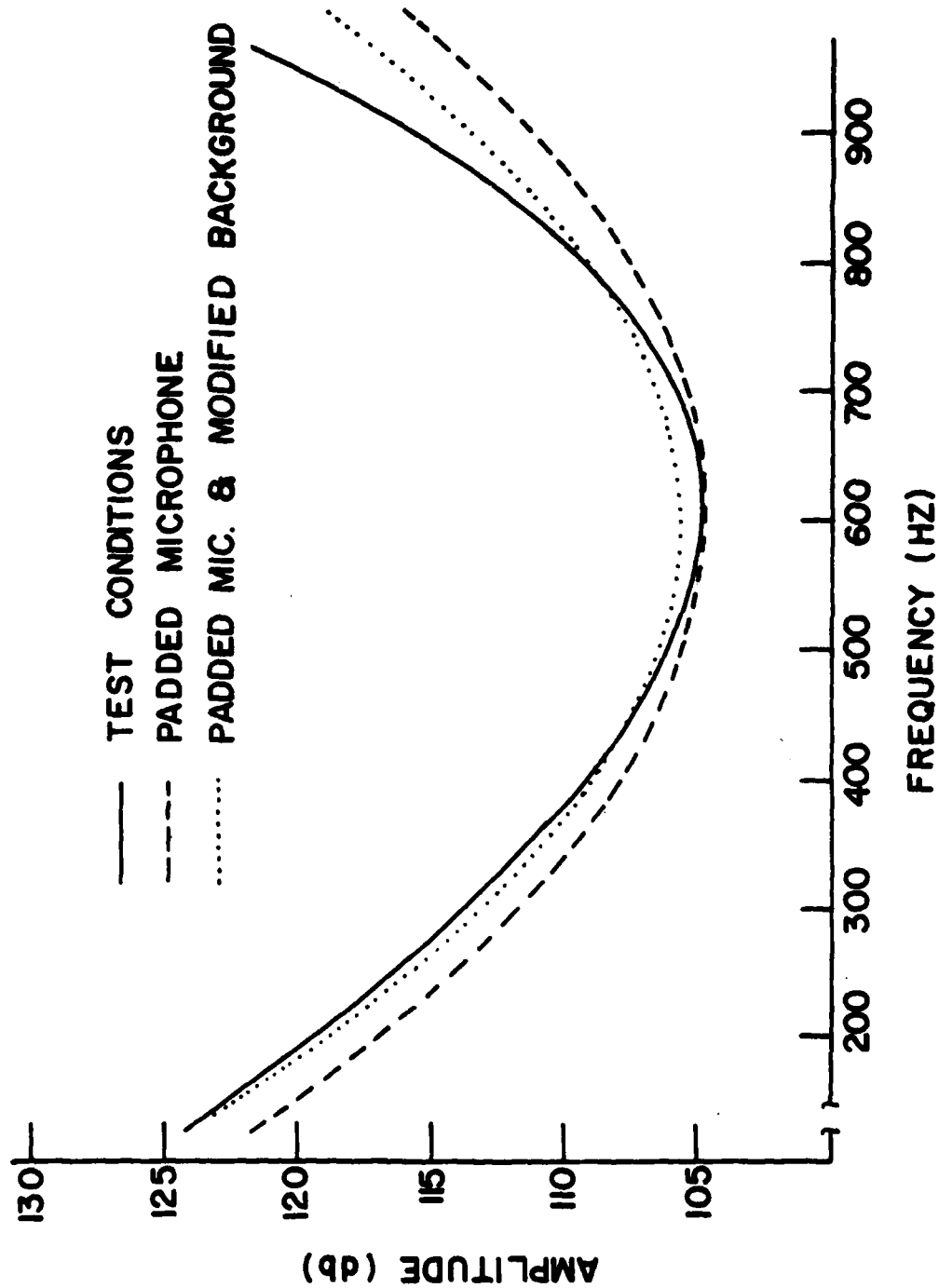FIGURE 16. NOISE INTENSITY VS. FREQUENCY, RUNS 3 AND 3a

DISTRIBUTION LIST

No. of Copies

1. Library   2
   Code 0142
   Naval Postgraduate School
   Monterey, CA 93940

2. Department of Aeronautics
   Code 67
   Naval Postgraduate School
   Monterey, CA 93940
      M. F. Platzer, Chairman   1
      D. W. Netzer   10

3. Dean of Research   1
   Code 012
   Naval Postgraduate School
   Monterey, CA 93940

4. Defense Documentation Center   2
   Cameron Station
   Alexandria, VA 22314

5. Chief of Naval Operations   2
   Navy Department
   Washington, DC 20360
   (Attn: Code: OP451, OP453)

6. Chief of Naval Material   2
   Navy Department
   Washington, DC 20360
   (Attn: Codes: 08T241, 044P1)

7. Commander   8
   Naval Air Systems Command
   Washington, DC 20361
   (Codes: AIR-01B, 330D, 340E, 4147A,
   50184, 5341B, 53645, 536B1

8. Commanding Officer   1
   Naval Air Rework Facility
   Naval Air Station North Island
   San Diego, CA 92135
   Code: 64270

9. Commander   2
   Naval Facilities Engineering Command
   200 Stovall Street
   Alexandria, VA 22332
   (Codes: 104, 032B)

10. Naval Construction Battalion Center   3
    Port Hueneme, CA 93043
    (Codes: 25, 251, 252)

11. U. S. Naval Academy   1
    Annapolis, MD 21402
    (Attn: Prof. J. Williams)

12. Arnold Engineering Development Center   1
    Arnold AFS, TN 37342
    (Code: DYR)

13. Air Force Aero Propulsion Laboratory   1
    Wright-Patterson AFB, OH 45433
    (Code: SFF)

14. Detachment 1   2
    (Civil & Environmental Engineering
      Division Office)
    HQ ADTC (AFSC)
    Tyndall AFB, FL 32401
    (Code: EV, EVA)

15. Army Aviation Systems Command   1
    P.O. Box 209
    St. Louis, MO 63166
    (Code: EQP)

16. Eustis Directorate   1
    USA AMR & DL
    Ft. Eustis, VA 23604
    (Code: SAVDL-EU-TAP)

17. National Aeronautics and Space Admin.   1
    Lewis Research Center
    2100 Brookpark Road
    Cleveland, OH 44135
    (Attn: Mail Stop 60-6 (R. Rudley))

18. Federal Aviation Administration   1
    National Aviation Facility Experimental Ctr.
    Atlantic City, NJ 08405

19. Naval Air Propulsion Center   3
    Trenton, NJ 08628
    (Code PE71:AFK)

20. Naval Ocean Support Center   2
    271 Catalina Boulevard
    San Diego, CA 92152
    (Attn: M. Lepor, M. Harris; Code 5121)